Supporting Information

Beyond electronic effects: hydrogen-bond engineering via N-mediated microenvironment control for accelerated oxygen electroreduction

Wenhui Jiang,[a] Bingyu Huang,[a] Zhi Cai,[a] Binbing Tang,[b] Dirk Lützenkirchen-Hecht,[c] Kai Yuan,*[a] Yiwang Chen*[a,d]

a. College of Chemistry and Chemical Engineering/Film Energy Chemistry for Jiangxi Provincial Key Laboratory (FEC)/Institute of Polymers and Energy Chemistry (IPEC); Nanchang University, Nanchang 330031, China

E-mail: kai.yuan@ncu.edu.cn (K. Yuan), ywchen@ncu.edu.cn (Y. Chen).

b. School of Physics and Materials Science, Nanchang University, Nanchang 330031, China.

c. Faculty of Mathematics and Natural Sciences-Physics Department, Bergische Universität Wuppertal, D-42119 Wuppertal, Germany.

d. College of Chemistry and Chemical Engineering, Gannan Normal University, Ganzhou 341000, China.

Experimental Procedures

Materials and methods

Materials

Pyrazine-2,5-dicarbaldehyde (PZ-CHO, 95%) and pyridine-2,5-dicarbaldehyde (PD-CHO, 97%) were purchased from Bide Pharmatech Ltd. 1,4-phthalaldehyde (BDA, 98%), pyrrole (99%), trifluoroacetic acid (TFA, 99%) and nitrobenzene (NBZ, 99%) were purchased from Energy Chemical Co. Ltd. Potassium hydroxide (KOH) was purchased from Sinopharm Chemical Reagent Co. Ltd (China). Propionic acid was bought from Alfa Aesar. BLACK PEARLS 2000 (BP2000) was purchased from Cabot Corporation. Carbon paper was obtained from Hesen Electric Inc. Shanghai. Zinc foil was obtained from Tengfeng Metal Co., Ltd. All the reagents and solvents are analytical grade and used without further purification.

Materials Synthesis

Preparation of PZ-POP-Co

First, pyrazine-2,5-dicarbaldehyde (28 mg, 0.2 mmol) was dissolved into a mixture solution with 5 mL propionic acid, 20 μL TFA, and 10 μL NBZ under ultrasonic treatment for 30 min to form a homogenous suspension. After that, 32 μL pyrrole was added, then the as-obtained mixture was kept at 130 °C under constant magnetic stirring condition for 2 h to form a porphyrin-based polymer skeleton. The cobalt acetate equivalent to porphyrin moiety was dispersed in 6 mL propionic acid and added dropwise to the above solution under stirring. The mixture was kept at 130 °C for another 22 h, then cooled to room temperature (~25 °C) to provide a dark suspension. The suspension was filtrated, then washed with chloroform, deionized water and ethanol to remove unreacted reagents and porphyrin molecules. After vacuum drying at 60 °C overnight, the product (10 mg) and BP2000 (10 mg) were well mixed by grinding in agate mortar containing agate balls and 1 mL methanol under air atmosphere. The grinding bowl was later set into the ball mill and revolved for 12 h at 300 rpm. After separating the grinding beads, the obtained PZ-POP-Co was washed with deionized water and ethanol for three times. After vacuum drying at 60 °C overnight, PZ-POP-Co nanocomposite was obtained.

Preparation of PD-POP-Co and BDA-POP-Co

As comparison, PD-POP-Co and BDA-POP-Co were prepared using a similar synthesis process as PZ-POP-Co, but replacing pyrazine-2,5-dicarbaldehyde with pyridine-2,5-dicarbaldehyde and 1,4-phthalaldehyde, respectively.

Instrumentations

SEM measurements were performed via a scanning electron microscope (JEOL JSM-7900F). TEM images, HRTEM images, SAED patterns, EDS and HAADF STEM were obtained by employing a scanning transmission electron microscope (JEOL, JEM-2100F). The AC HAADF-STM measurement was performed by a scanning transmission electron microscope (Titan Cubed Themis G2 300). FT-IR spectra were recorded on a Thermo Scientific Nicolet 6700. The nitrogen adsorption-desorption measurements were performed on an Autosorb iQ (Anton-Paar China), and the specific surface areas were obtained by the BET model. XRD patterns were obtained by a Bruker 102 D8Discover 25 X-ray diffractometer. XPS spectra were recorded on a Kratos AXIS Ultra using monochromatized Alα-radiation. Zeta potential measurements were performed on a NanoBrook 90Plus PALS (Brookhaven Instruments Corporation, USA) at 25 °C. Ultraviolet-visible (UV-vis) absorption spectra were recorded on an Agilent series UV-vis-NIR spectrophotometer. Fluorescent quantum lifetimes were measured by fluorescence lifetime system (Light-Stone Instruments NTASTCSPC). Magnetic susceptibility was measured in a Quantum Design PPMS-9T.

Electrochemical measurements

Electrochemical characterization was performed on AutoLab PGSTAT302Nl with PINE AFMSRCE. The electrocatalyst was loaded on a rotating disk electrode (RDE) (disk area: 0.196 cm^2) or a rotating ring-disk electrode (RRDE) (disk area: 0.1866 cm^2, ring area: 0.2475 cm^2) as working electrode. Graphite rod was used as counter electrode, Ag/AgCl electrode and 0.1 M KOH aqueous solution were used as counter electrode, reference electrode and electrolyte, respectively. Before each test, the electrocatalyst ink was prepared by sonicating a mixture of 5 mg electrocatalyst, 500 μL isopropyl alcohol, and 50 μL of 5 wt% Nafion solution for 1 h. Next, 10 μL of the catalyst ink was deposited on a glassy carbon electrode and dried at room

temperature. Linear sweep voltammetry (LSV) curves were recorded at 225–2025 rpm with a sweep rate of 10 mV s^{-1} using RDE. All LSV measurements were performed with automatic iR compensation set at 85% to minimize ohmic drop and ensure accurate potential reporting. The electron-transfer number (n) was calculated from the Koutecky-Levich (K-L) equation, which is expressed as follows:

$$\frac{1}{j}=\frac{1}{j_L}+\frac{1}{j_K}=\frac{1}{\frac{1}{B\omega^{\frac{1}{2}}}}+\frac{1}{j_K}$$

Here, j is the measured current density, j_K and j_L are the kinetic-limiting and diffusion limiting current densities, respectively, ω is the electrode rotating speed in rad s^{-1}, the K-L plots ($\omega^{-1/2}$ vs j^{-1}) in O_2-saturated 0.1 M KOH can be come from LSV curves at various rotation speeds. B can be determined from the slope of K-L plots as given by

$$B = 0.62nFC_0(D_0)^{2/3}v^{-1/6}$$

where F is the Faraday constant (F= 96485 C mol^{-1}), C_0 is the bulk concentration of O_2 in 0.1 M KOH (1.2 × 10^{-6} mol cm^{-3}), D_0 is the diffusion coefficient of O_2 in 0.1 M KOH (1.9 × 10^{-5} cm^2 s^{-1}), and v is the kinetic viscosity of 0.1 M KOH (0.01 cm^2 s^{-1}).

The transferred electrons number (n) was determined by RRDE measurements. The HO_2^- (%) and the n were calculated by the following equations:

$$\left(HO_2^-\right)\% = \frac{200 \times I_{Ring}}{I_{Ring} + I_{Disk} \times N}$$

$$n = \frac{4 \times I_{Disk}}{I_{Disk} + I_{Ring}/N}$$

where I_D is the disk current, I_R is the ring current, and N (= 0.37) is the collection efficiency of RRDE.

The ECSA was determined by measuring the capacitive current associated with double-layer charging from the scan rate dependence of the CV. This measurement was performed on the same working electrode in a potential window of 1.00-1.10 V vs. RHE and scan rates ranging from 1.0 to 10.0 mV s^{-1}. Then, linear fitting of the charging current density differences ($\Delta j = j_a - j_c$ at a potential of 1.05 V vs. RHE) against the scan rate was done. j_a and j_c represent the anodic and cathodic current densities, respectively. The slope is twice the double layer capacitance C_{dl}. ECSA was calculated using ECSA=$R_f/m_{loading}$, where $m_{loading}$ is the loading

mass of catalyst per geometrical area of the electrode. $R_f = C_{dl}/40$ μF cm^{-2} (the average specific capacitance of a flat standard electrode with 1 cm^2 of real surface area is 40 μF cm^{-2}). The EIS measurements were recorded in the frequency range from 100 kHz to 0.1 Hz with an AC signal amplitude of 10 mV in an N_2- saturated 0.1 M KOH electrolyte.

Electrochemical impedance spectroscopy (EIS) and distribution of relaxation times (DRT) analysis

EIS tests were performed on the AutoLab (PGSTAT302Nl). Operando EIS for ZABs was carried out from 100 kHz to 0.05 Hz under different discharge current densities, with 10 points per decade and 2 mA amplitude. DRT was calculated based on EIS data (discarding inductive data) by MatlabR2022 with a freely available toolbox of *DRT-TOOLS* developed by Prof. Francesco Ciucci1 team.[1] The regularization parameter λ is set to 10^{-3}, and the Full Width at Half Maximum (FWHM) factor is 0.5.

O_2 adsorption capability assessment

The oxygen adsorption capacity of as-prepared catalysts was accessed by chronoamperometry. Two electrolytic cells were filled with 0.1 M KOH, one was saturated with O_2, while the other was purged with N_2 to remove dissolved oxygen. The working electrode loaded with catalyst was first immersed in the O_2-saturated electrolyte to adsorb oxygen on active sites. It was then quickly transferred to the O_2-free electrolyte, chronoamperometry was performed at an applied potential of 0.4 V_{RHE}, where the adsorbed O_2 can be consumed. Control experiments were performed between two O_2-free electrolytic cells to eliminate capacitive contributions. The chronoamperometric *I-t* curves with "-O_2^{ad}" suffix represent for oxygen adsorption tests, and those with "-N_2" suffix represent for control experiments. The O_2 adsorbance was calculated by following equation:

$$Adsorbance = \frac{Q_{-O_2^{ad}} - Q_{-N_2}}{F \times n \times m_{cat.}}$$

where $Q_{-O_2^{ad}}$ and Q_{-N_2} is the integrated charge of chronoamperometric *I-t* curves with corresponding suffix. *F* is Faraday's constant (96485 C mol^{-1}). *n* is the average electron transfer number calculated from RRDE tests. The *n* of carbon black (CB) was assumed to be 4.

The measurement method for PZC.

Differential capacitance was measured to obtain the PZC of working electrodes using AutoLab PGSTAT302Nl with PINE AFMSRCE. The frequency range was 10^5 Hz-0.05 Hz, and the amplitude was 5 mV. The double-layer capacitance (C_{dl}) was calculated from the constant phase element (CPE) parameters and the two resistances using the following Brug formula:

$$C_{dl} = T^{\frac{1}{P}}\left(\frac{1}{R_S} + \frac{1}{R_{ct}}\right)^{\frac{P-1}{P}}$$

where R_s is the solution resistance, R_{ct} is the charge transfer resistance, *T* is the CPE constant, and *P* is the CPE exponent. We used the equivalent circuit of Figure S28 to simulate the experimental data points. The relevant parameter values were fitted by ZView2 software.

Proton conductivity measurement.

Proton conductivity of the X-POP-Co were carried out via the AC electrochemical impedance spectroscopy method with a frequency from 0.1 Hz to 7 MHz and an amplitude of 10 mV at a potential of 0 mV (vs. RHE), using a CHI660E workstation. About 30 mg of X-POP-Co were pressed into circular pellets (16 mm in diameter, 0.2 mm in thickness) under a pressure of 5 MPa for 5min.

The semicircle with characteristic strays at low frequencies indicates the blocking of protons at the electrode. Proton conductivity was calculated by using the following formula:

$$\sigma = \frac{L}{Z \times d \times w}$$

where σ is the conductivity (S cm^{-1}), *L* is the thickness of the measured plate (cm), *Z* is the measured impedance (Ω), *d* is width of electrodes overlap area, and *w* is the width of electrode. The activation energy (E_a) is calculated by using the conductivity data at 98% RH with the Arrhenius equation:

$$\ln(\sigma T) = lnA - \frac{E_a}{k_B T}$$

where k_B and *A* are the Boltzmann constant and the pre-exponential factor, respectively.

Scanning electrochemical microscope (SECM)

The SECM measurements were performed on a CHI920D, including a bipotentiostat and a high-resolution 3D electrode positioner. The probe was a CHI116 10 μm Pt SECM tip. The substrate was a homemade concave Au electrode with a recessed microdisk with diameter of 25 μm at the depth of ~7 μm. An Ag/AgCl electrode was used as reference electrode. A Pt wire was used as counter electrode. The electrolyte was Ar- saturation 0.1 M KOH aqueous solution with 0.5 mM FcMeOH.

The processing of substrate was following the literatures. In brief, a 25 μm Au wire was inserted into a glass capillary tube (outer diameter of 2.2 mm), then heating with an oxyhydrogen flame to sealing the Au wire into the tube. A copper wire was attached on one side of Au wire by silver conductive paint. The end of the capillary containing the sealed Au wire is polished flat with successively finer grit sandpaper (400-, 600-, 800-, 1000-, 3000-grit) until the exposure of Au surface. Then the polished electrode was electrochemically etched in the $CaCl_2$ solution to dig a cavity. An optical microscope was used to check the sealing and the depth of cavity. To load catalysts into concave electrode, catalyst powder was spread onto the surface of glass slide. Then, gently pressing the concave electrode onto the catalyst powder along vertical direction, and wiping the residuals with a lens wiping paper. An optical microscope was used to check the loading and flatness. The procedure may repeat several times, until the cavity is filled with catalyst powder.

Probe approach curve technique was used to positioning z axis and adjusting platform. The probe was biased at 0.5 $V_{Ag/AgCl}$ to oxide FcMeOH to $FcMeOH^+$. When the probe approaching very close to the surface of substrate, the feedback current will be greatly changed due to the restricted diffusion. A cut off set at a current level of 75 % to avoid crash. A quiet time set for 20 s to steady current value. The adjustment of platform was based on three-point fix method.

SECM technique was used to locating the catalyst region. The probe was biased at 0.85 $V_{Ag/AgCl}$ and the substrate was biased at - 0.9646 $V_{Ag/AgCl}$. Firstly, a 500 × 500 μm scan (5 μm/step) was performed for rough locating. Subsequently, a 200 × 200 μm scan (2 μm /step) was performed for fine positioning. The probe returned back to origin when the measurement finished. A quiet time set for 20 s to steady current value. The TG/SC mode SECM images were recorded on this

200 × 200 μm region, but changing a series of the given substrate bias potential ranged from -0.9646 $V_{Ag/AgCl}$ to -0.0646 $V_{Ag/AgCl.}$

Surface-interrogation (SI-) SECM measurement

The SI-SECM was performed on the same platform as SECM. Firstly, the C_{dl} was measured by a series of CV scanning in a non-Faradaic potential (0.05 - 0.15 V vs. RHE) at given scan rates of 10, 20, 30, 40, 50 mV s^{-1}. The $ECSA_{UME}$ (subscript UME is to declare the data obtained from ultra-micro electrode) was determined by the same procedure as described in previous electrochemical measurements section.

Subsequently, the Pt tip was electrochemically cleaned by CV cycling from -0.9646 $V_{Ag/AgCl}$ to -0.4646 $V_{Ag/AgCl}$ at 50 mV s^{-1} for ~300 s. Then, the probe was switched to open circuit and the substrate was subject to given bias potential from -0.9646 $V_{Ag/AgCl}$ to 0.2354 $V_{Ag/AgCl}$ for 30 s. After that, the substrate was immediately switched to open circuit, while the probe was biased at 0.4 $V_{Ag/AgCl}$ for 30 s. The feedback current at probe (I_{tip}) was recorded. The electric quantity at tip (Q_{tip}) was derived by background subtraction and integration of I_{tip}. The active site density (SD) was followed the relation as described by following equation:

$$SD = \frac{Q_{tip}/F \times N_A}{ECSA_{UME}}$$

where F represents the Faraday's constant (96485 C mol^{-1}) and N_A is the Avogadro constant (6.02×10^{23} mol^{-1}).

The turnover frequency (TOF) was calculated by following equation:

$$TOF = \frac{N_A \times j_m}{SD_{mass} \times F}$$

The kinetic mass activity (j_m) for the as-papered catalysts in this work is defined as:

$$j_m = \frac{j_K}{m_{catalyst}}$$

where $m_{catalyst}$ is the catalyst loading on the glassy carbon disc (mg cm^{-2}), the potential to determine kinetic current density (j_k) is chosen at 0.8 V.

XAFS measurements

X-ray absorption spectroscopy (XAS) experiments were carried out at the wiggler beamline BL10 at the DELTA storage ring (Dortmund, Germany) operated with 80-130 mA of 1.5 GeV

electrons. Co K-edge spectra were collected using a Si (111)-channel cut monochromator and gas-filled ionization chambers as detectors for the incoming and the transmitted intensities, and a large area photodiode for the fluorescence photons.

Laviron equation

$$E_c = E_{1/2} - (\frac{RT}{\alpha nF}) \times \ln\left(\frac{RT}{RTk_s}\right) - (\frac{RT}{\alpha nF}) \times \ln(v)$$

where E_c is the reduction potential of metal redox, $E_{1/2}$ is the formal potential of metal redox, R is the universal gas constant, T is the temperature in kelvin, n is the number of electrons transferred, α is the transfer coefficient, k_s is the kinetic constant of metal redox, and v is the scan rate in the CV measurement.

VF-SWV measurements

Square wave voltammetry tests were performed in N_2-saturated 0.1 M KOH electrolyte with a step potential of 10 mV, amplitude of 25 mV. The perturbation frequency (f) was varied from 1250 to 0.33 Hz.

Electron transfer reaction between catalysts and TCNQ

5 mg of catalyst was exposed to 5 mL 7.65 mM TCNQ acetonitrile solution in a centrifuge tube through ultrasonic treatment, followed by stirring the suspension at 70 °C for 20 min to accelerate the electron transfer reaction. Subsequently, the supernatant is separated by centrifugation for further analysis by UV-vis absorption spectra. The original TCNQ solution was diluted 250-fold with acetonitrile before measurement. The TCNQ solution reacted with the catalyst and was diluted twofold with acetonitrile before the measurements.

Aqueous ZAB assembly and testing

An in-house-developed aqueous ZABs were built and assembled to evaluate the electrochemical energy conversion performance of the composite materials. It was constructed by pairing X-POP-Co loaded onto a carbon paper (HCP020P, 0.19 mm thickness) with a Zn plate (0.20 mm thickness, 99.99% purity) in 6 M KOH (20 mL). The ZABs were assembled

applying the following procedure: First, the air electrodes were prepared by pipetting catalyst slurry carefully onto the carbon paper, the catalyst loading on carbon paper is ~120 μg (0.25 mg cm^{-2}). Subsequently, polished zinc plates served as the anode, zinc plates were manually polished with finer grit sandpaper (1000-, 2000-, 3000-grit) beforehand, followed by the sonication in deionized water for several minutes. Battery tests were carried out at room temperature (25 °C ± 2 °C) under a dry air atmosphere with a CHI 760E and a LAND CT2001A. The specific capacity and specific energy can be obtained from the consumed Zn after discharge.

Operando attenuated total reflection surface-enhanced infrared absorption spectroscopy (ATR-SEIRAS) was employed on a Thermo Scientific Nicolet iS50 with a liquid-nitrogen-cooled MCT detector. During the test, the catalyst was loaded onto the surface of a silicon prism with an Au film as the working electrode, Pt foil as the counter electrode and Ag/AgCl electrode as reference electrode, respectively. The test potential ranges from 0.4 to 1.0 V vs. RHE in O_2-saturated 0.1 M KOH solution.

Computational Details

All the calculations are performed in the framework of the density functional theory with the projector augmented plane-wave method, as implemented in the Vienna ab initio simulation package.[2-3] The generalized gradient approximation proposed by Perdew-Burke-Ernzerhof (PBE) is selected for the exchange-correlation potential.[4] Electron spin polarization is taken into account in all calculations. The cut-off energy for plane wave is set to 450 eV. The energy criterion is set to 10^{-5} eV in iterative solution of the Kohn-Sham equation. All the structures are relaxed until the residual forces on the atoms have declined to less than 0.03 eV/Å. The Gamma cheme was utilized for Brillouin zone sampling, with a k-points mesh of 3 × 3 × 1.

The ORR pathways, involving OOH, *O, and *OH intermediates, were examined by calculating adsorption energies. The reaction Gibbs free energy (ΔG) was evaluated by accounting for zero-point energy, enthalpy, and entropy terms. The standard reference for the free energy of $H^+ + e^-$ was half the free energy of H_2.

$$\Delta G = \Delta E + \Delta ZPE - \Delta TS + \Delta G_U + \Delta G_{PH}$$

Here, e is the total system energy, ZPE denotes the zero-point energy, and S is the entropy. Zero-point-energy (ZPE) and entropy corrections were obtained from frequency calculations. The applied potential is represented by U, while ΔG pH serves as the pH-dependent free-energy correction for H^+. Under alkaline conditions, the overall ORR can be written as: $O_2+2H_2O+4e^- \longrightarrow 4OH^-$. This reaction involves a series of elementary steps, commonly used to illustrate the ORR electrocatalytic process on active sites.

$$O_2\ (g) + H_2O\ (l) + e^- + * \rightarrow {}^*OOH + OH^-$$

$${}^*OOH + e^- \rightarrow {}^*O + OH^-$$

$${}^*O + H_2O\ (l) + e^- \rightarrow {}^*OH + OH^-$$

$${}^*OH + e^- \rightarrow OH^-$$

where * represents the active site on catalytic surface, (l) and (g) stand for liquid and gas phases, respectively.

Ab initio molecular dynamics (AIMD) simulation was carried out to study disorder structures. During geometry optimization, the cut-off energy was set as 300 eV for structures, respectively. The Brillouin zone was sampled by a Monkhorst-Pack (MP) k-point grid of 1×1×1 for geometry optimizations. The conjugated gradient method was applied with a smearing width of 0.2 eV, and the convergence criteria for the energy and force were 10^{-5} eV/cell and 0.05 eV/Å, respectively. AIMD simulations were run for 2 ps as equilibration with time steps of 1 fs, performing a constant temperature of 300 K in the Nosé -Hoover isokinetic ensemble.

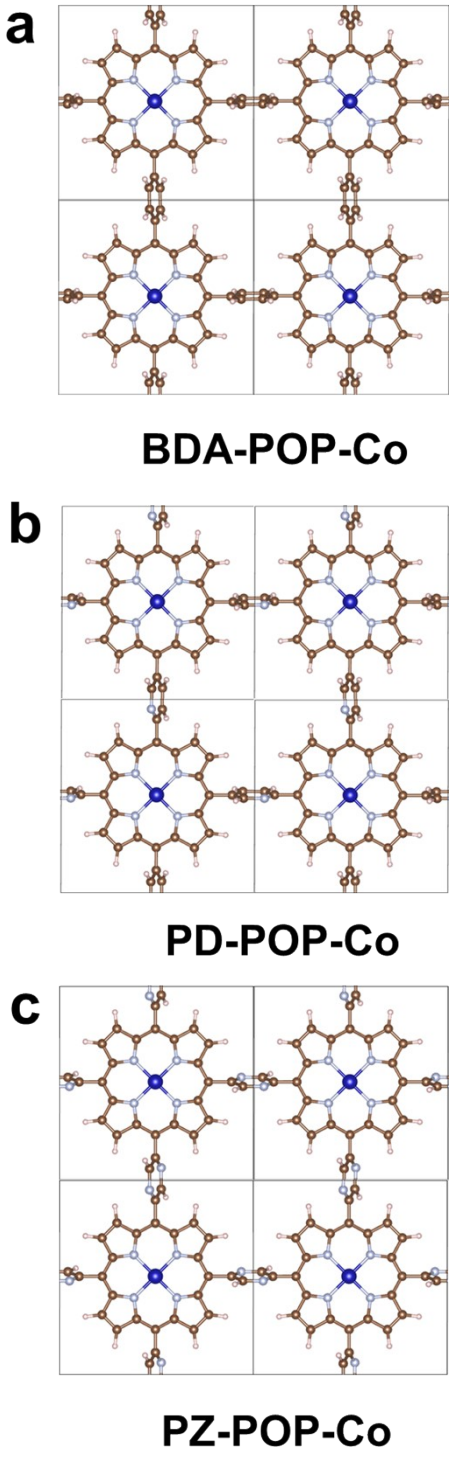

Figure S1. The theoretical computational models of (a) BDA-POP-Co, (b) PD-POP-Co and (c) PZ-POP-Co.

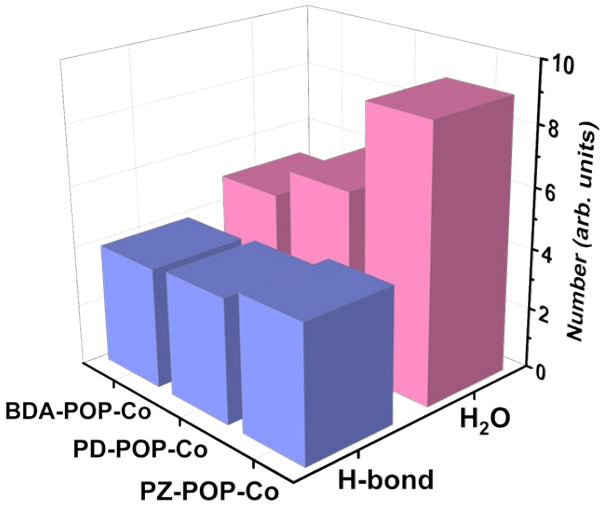

Figure S2. The average number of hydrogen bonds and corresponding H_2O molecules at different catalysts' interface.

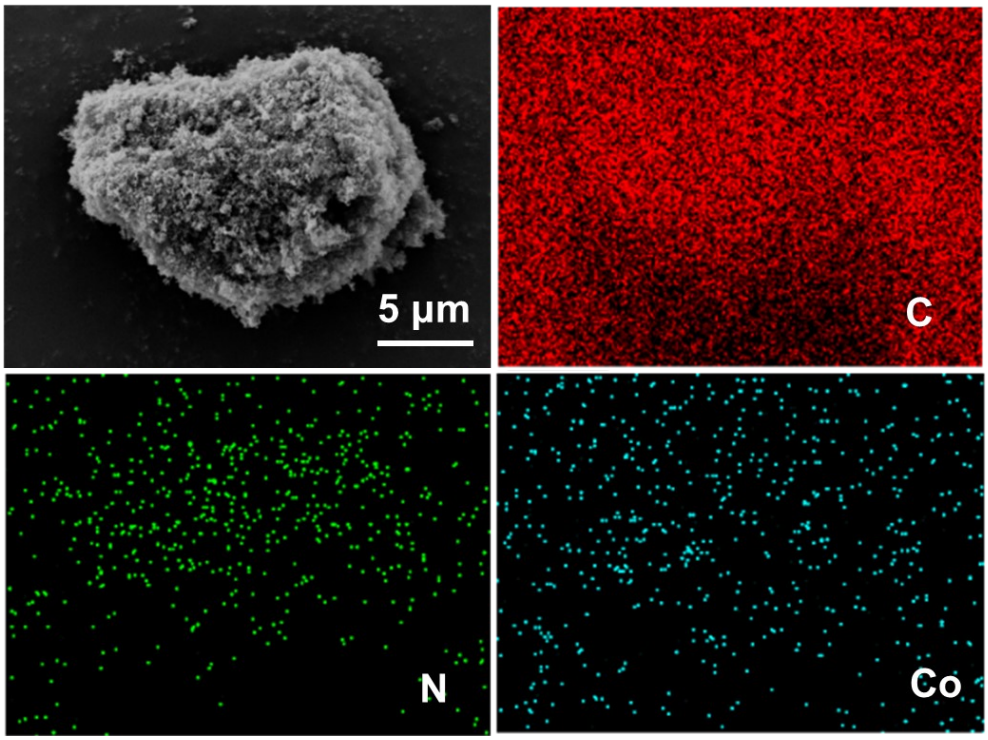

Figure S3. SEM image and corresponding EDS elemental mapping images of BDA-POP-Co.

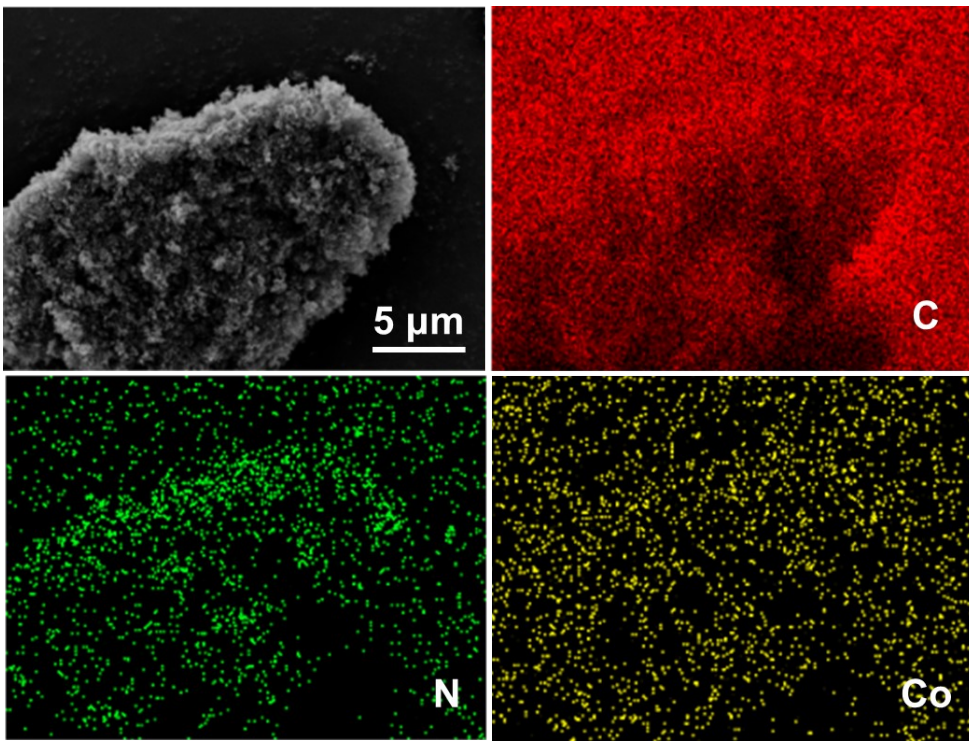

Figure S4. SEM image and corresponding EDS elemental mapping images of PD-POP-Co.

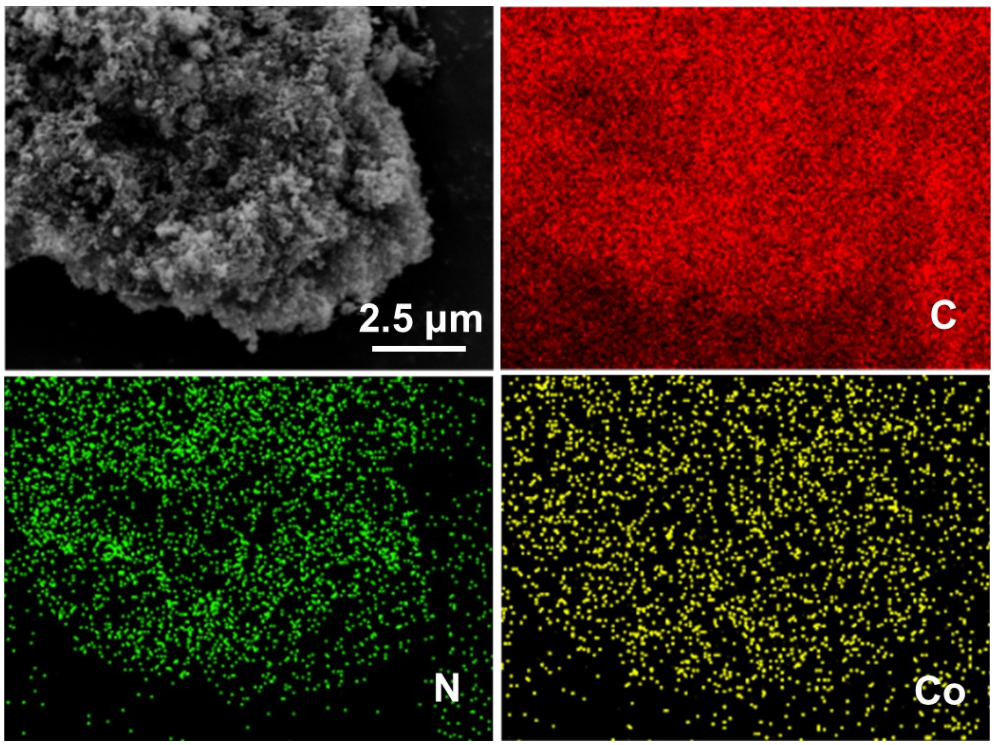

Figure S5. SEM image and corresponding EDS elemental mapping images of PZ-POP-Co.

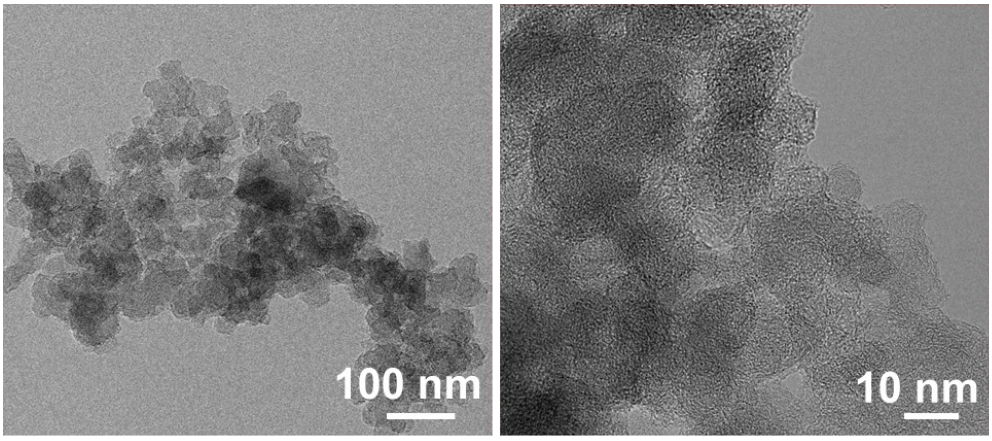

Figure S6. The TEM images with different magnifications of PZ-POP-Co.

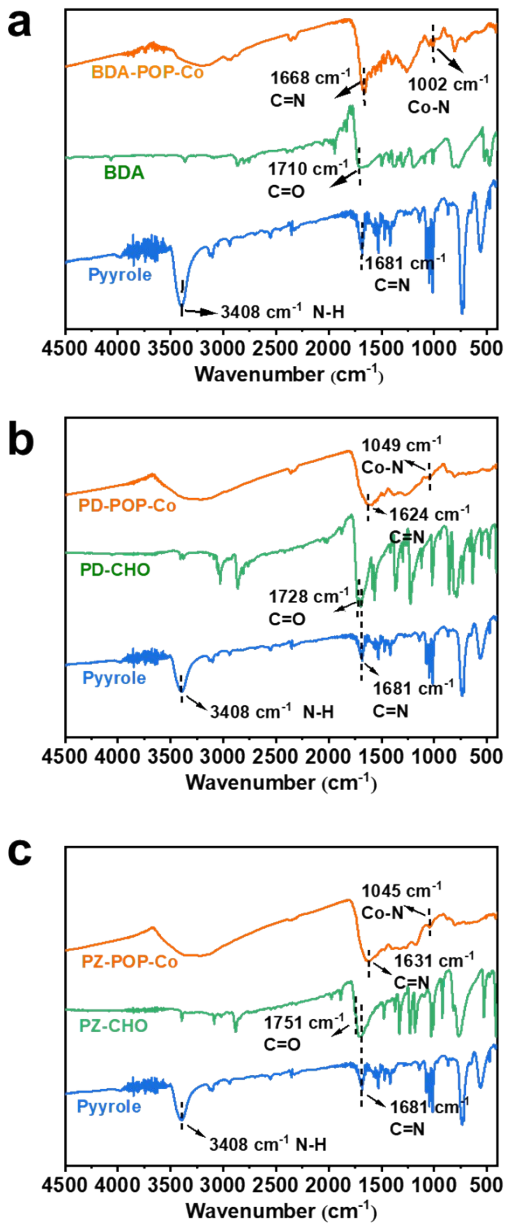

Figure S7. FT-IR spectra of **a** BDA-POP-Co, **b** PD-POP-Co, and **c** PZ-POP-Co and their monomers, including BDA, PD-CHO, PZ-CHO and pyrrole.

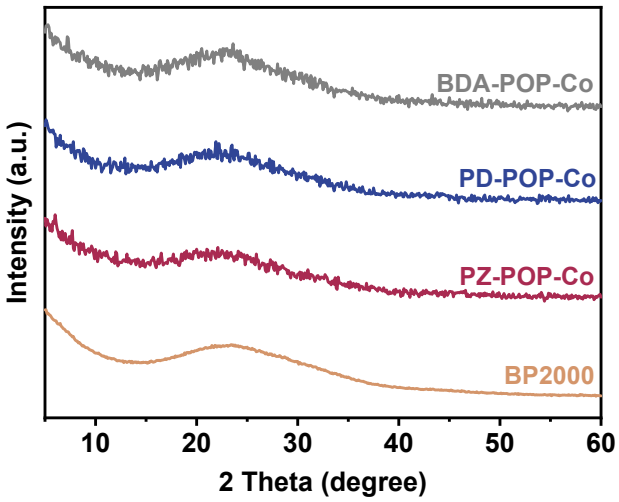

Figure S8. XRD patterns of BDA-POP-Co, PD-POP-Co, PZ-POP-Co, and BP-2000.

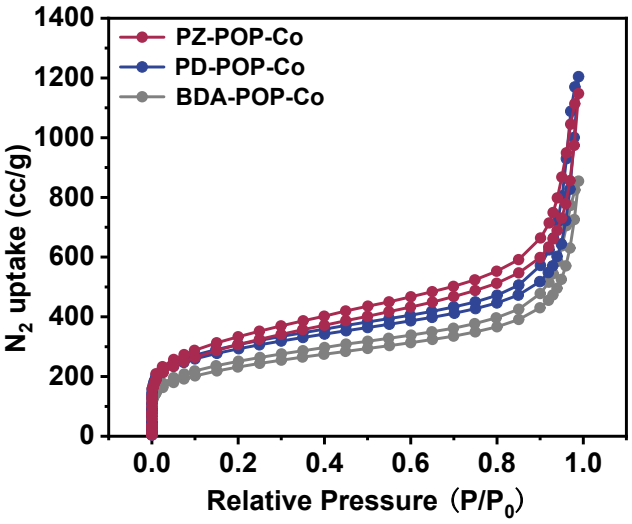

Figure S9. N_2 adsorption-desorption isotherms of X-POP-Co.

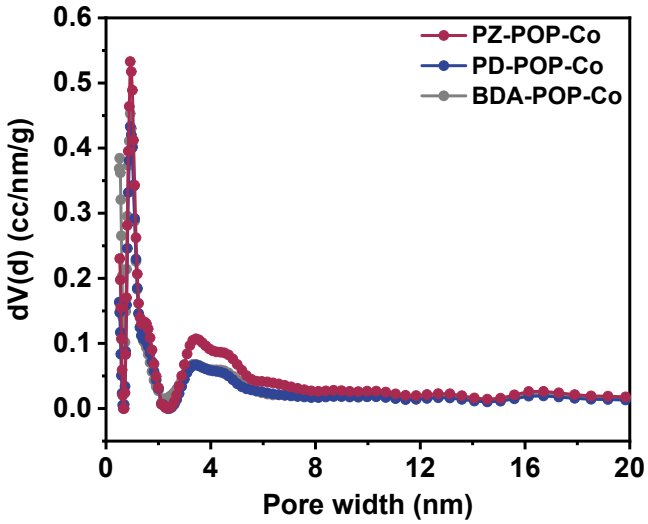

Figure S10. Pore size distribution profiles of X-POP-Co.

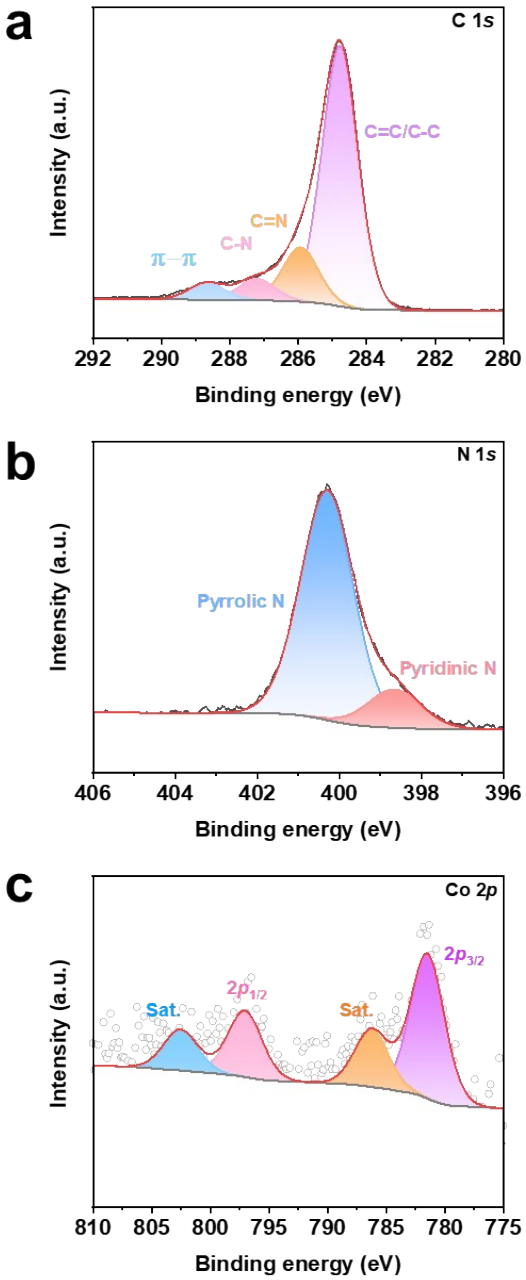

Figure S11. High-resolution **a** C 1*s*, **b** N 1*s* and **c** Co 2*p* XPS spectra of BDA-POP-Co.

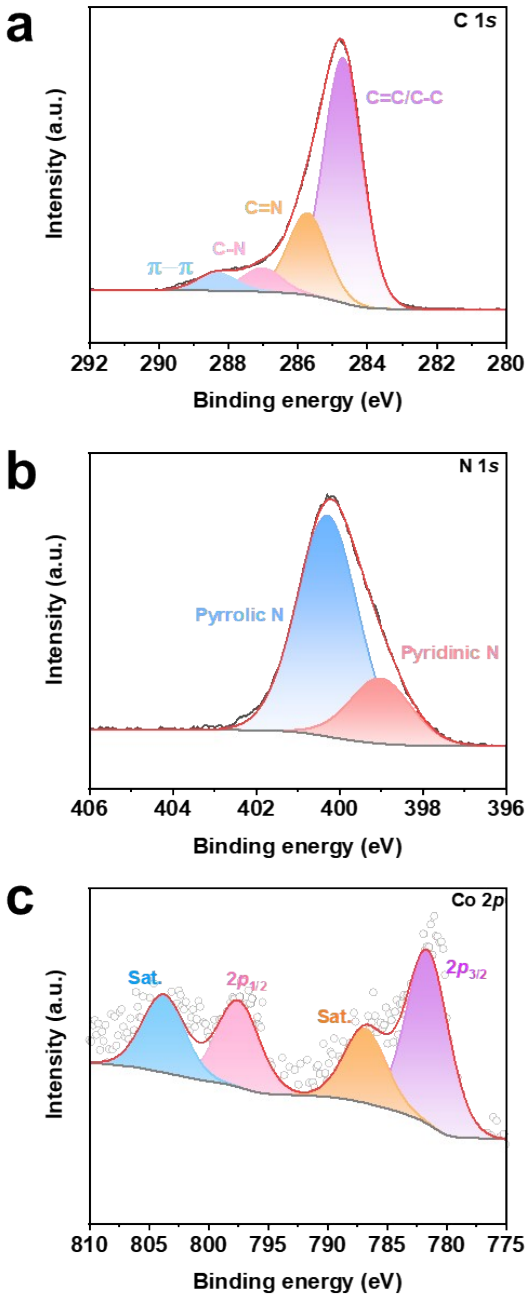

Figure S12. High-resolution **a** C 1*s*, **b** N 1*s* and **c** Co 2*p* XPS spectra of PD-POP-Co.

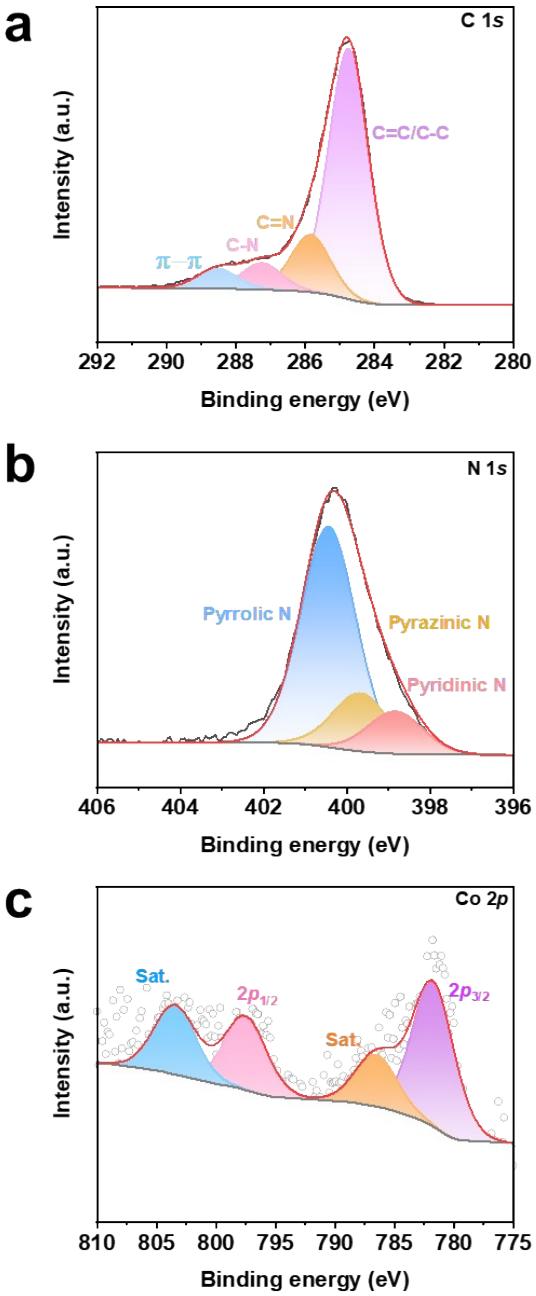

Figure S13. High-resolution **a** C 1*s*, **b** N 1*s* and **c** Co 2*p* XPS spectra of PZ-POP-Co.

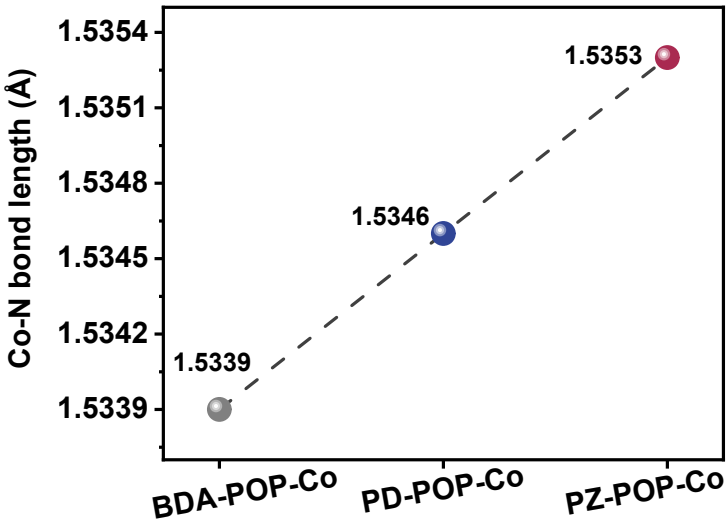

Figure S14. Co-N bond length for X-POP-Co.

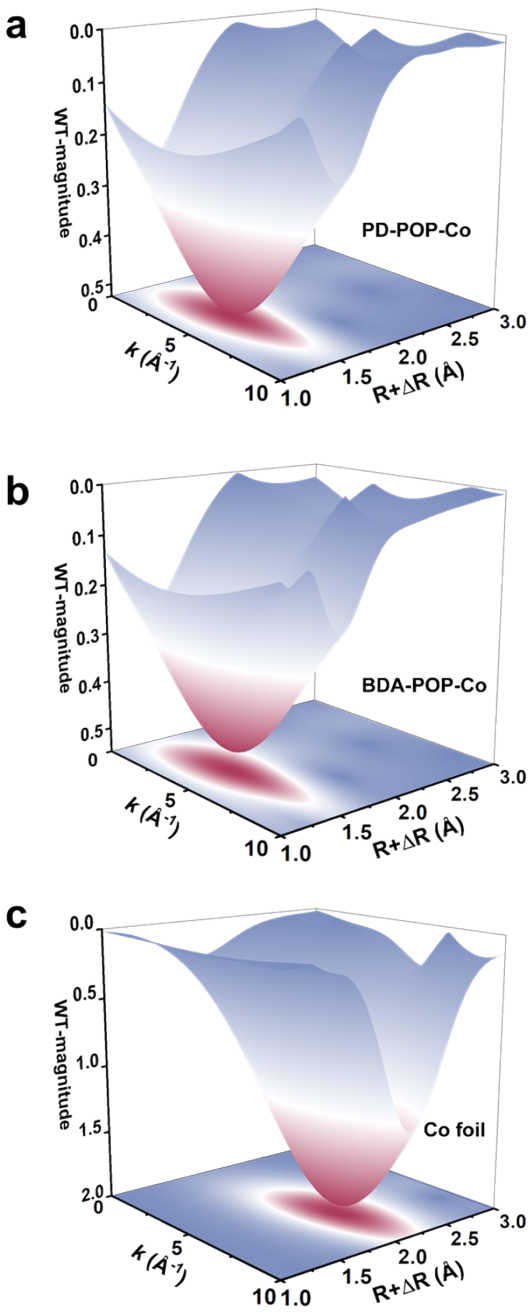

Figure S15. WT-EXAFS plots of **a** PD-POP-Co, **b** BDA-POP-Co and **c** Co foil.

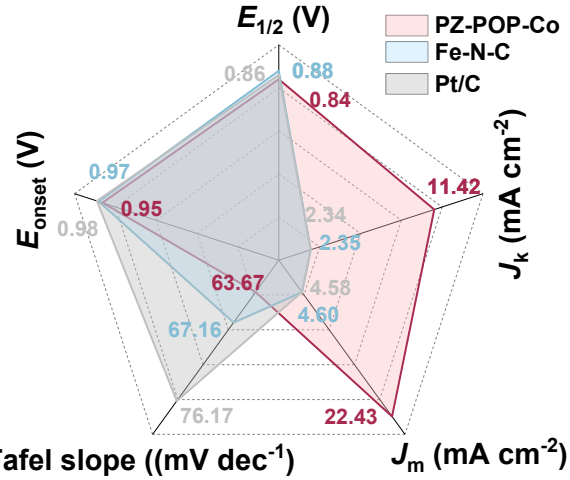

Figure S16. Comprehensive performance radar chart of $E_{1/2}$, E_{onset}, Tafel slope, J_k, and J_m (at 0.80 V) for PZ-POP-Co, Fe-N-C and Pt/C.

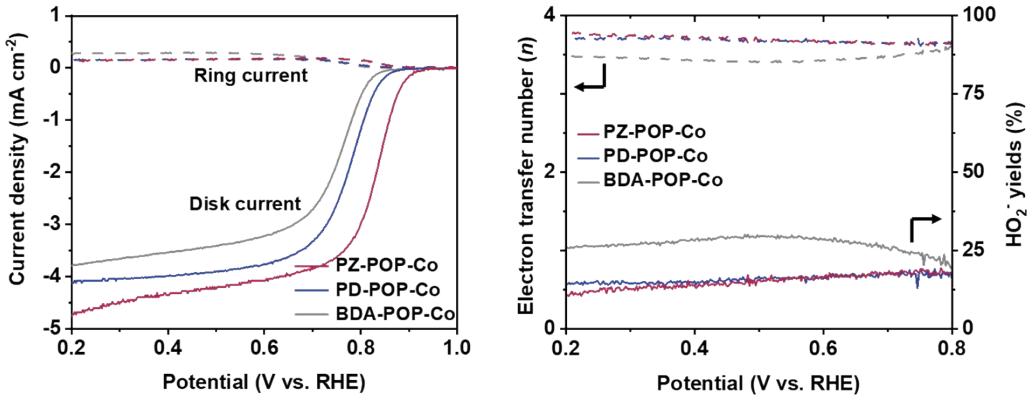

Figure S17. RRDE LSV curves and corresponding electron transfer number (*n*) and HO_2^- yield of X-POP-Co.

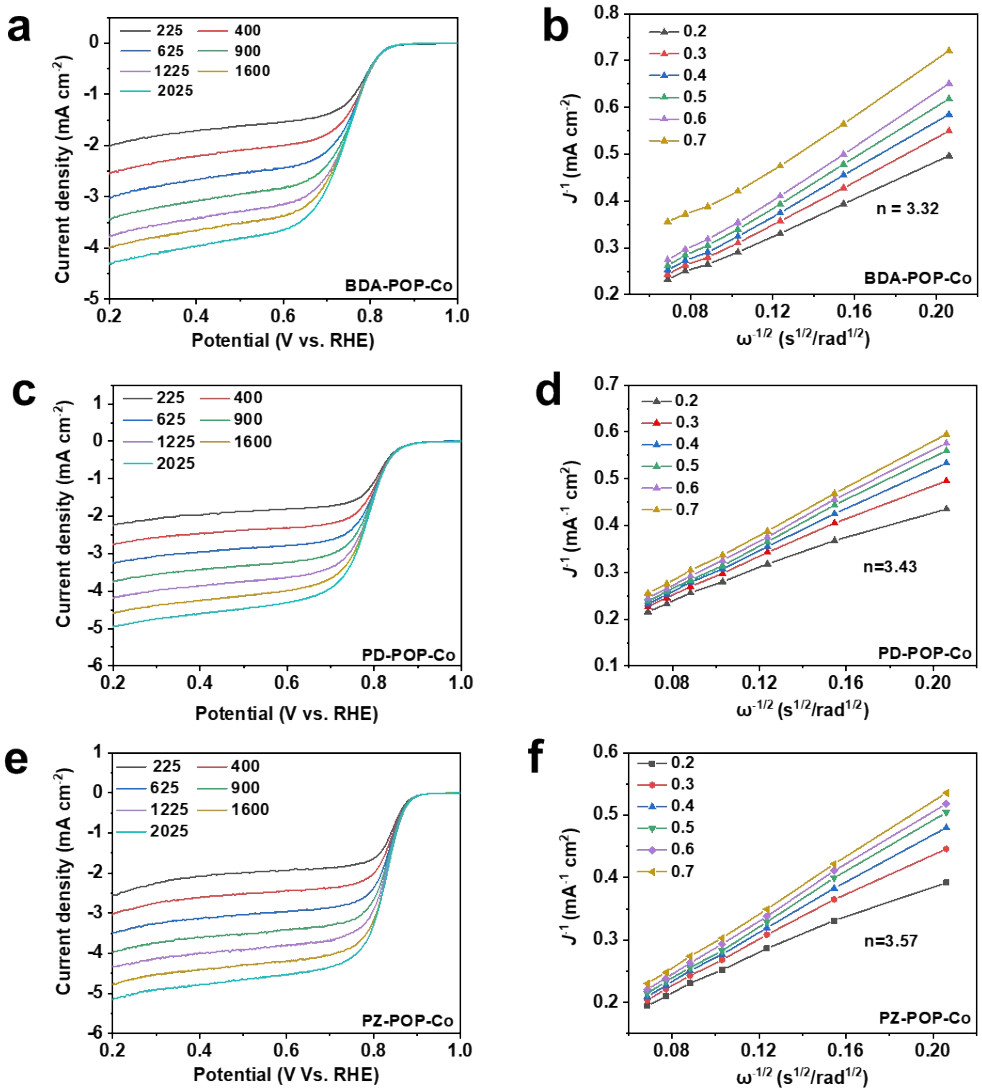

Figure S18. LSV curves at different rotation rates in 0.1 M KOH and corresponding K−L plots of **a, b** BDA-POP-Co, **c, d** PD-POP-Co, and **e, f** PZ-POP-Co.

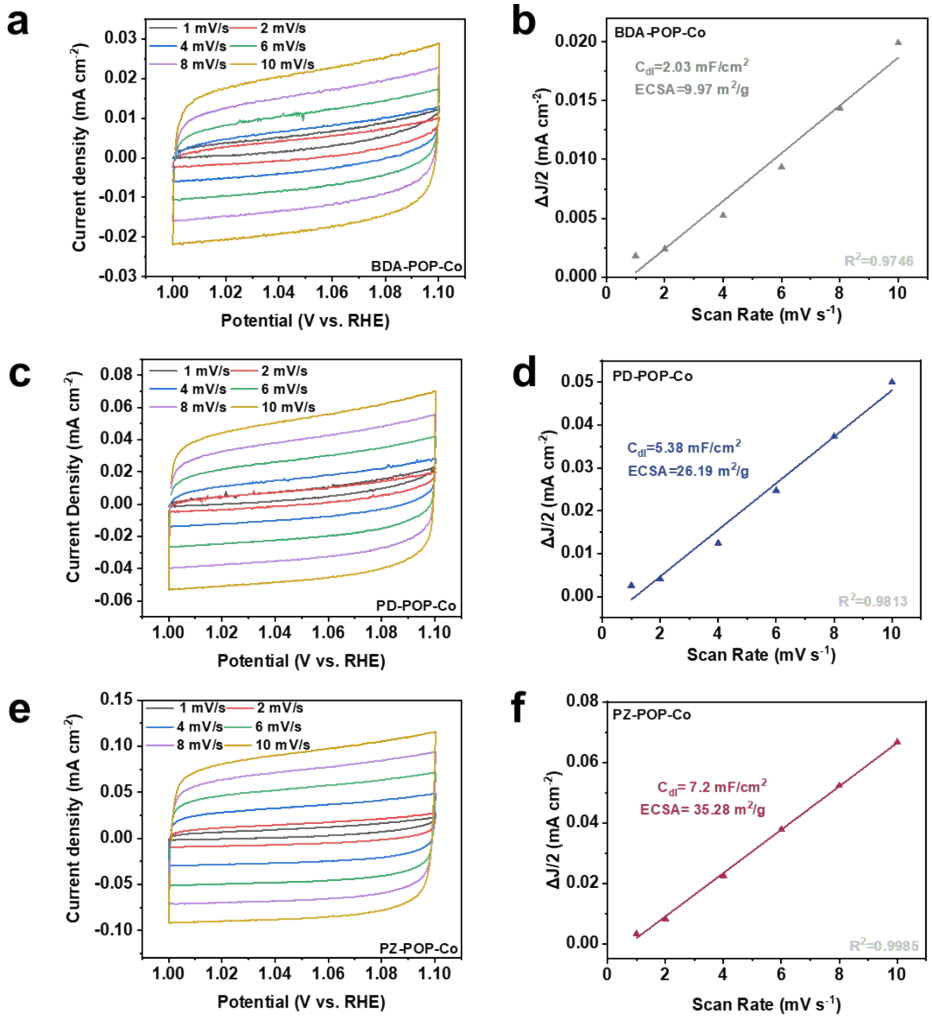

Figure S19. CV curves in the region of 1.0-1.1 V (vs. RHE) at various scan rates (left), the corresponding double-layer capacitance (C_{dl}) and ECSA (right) of **a, b** BDA-POP-Co, **c, d** PD-POP-Co, and **e, f** PZ-POP-Co at room temperature (~25 ℃).

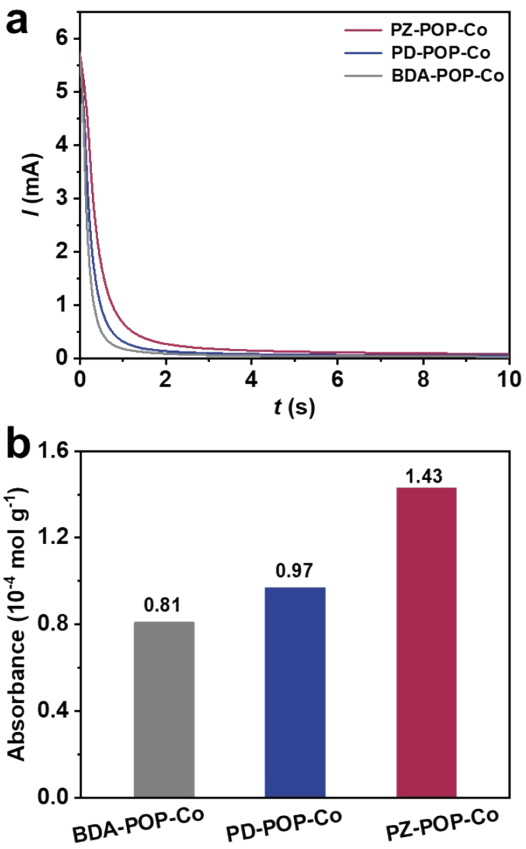

Figure S20. a Chronoamperometric *I-t* curves, and **b** O_2 absorbance for X-POP-Co.

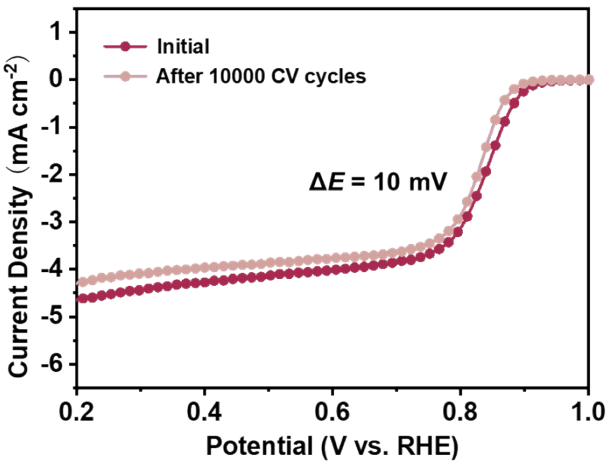

Figure S21. The LSV polarization curves of PZ-POP-Co before and after 10000 cycles.

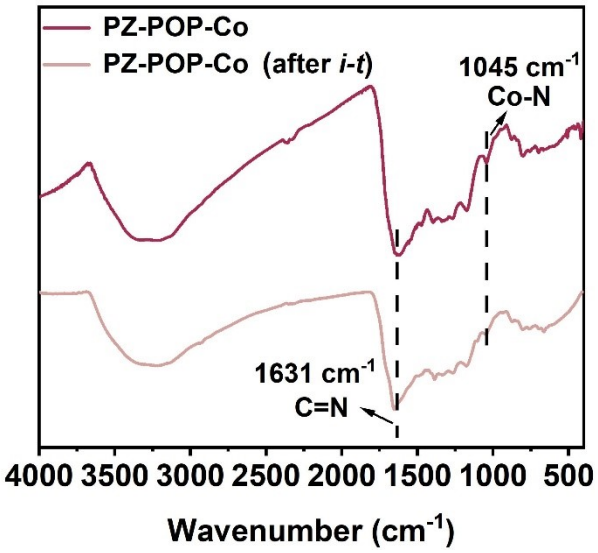

Figure S22. FT-IR spectra of PZ-POP-Co before and after *i-t* test.

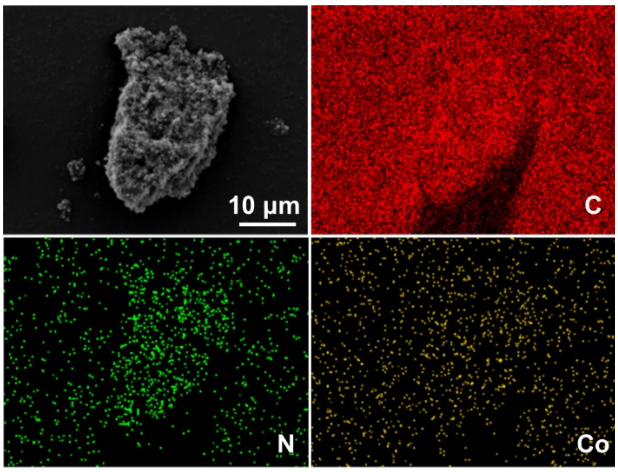

Figure S23. SEM and the corresponding EDS mapping images of PZ-POP-Co after *i-t* test.

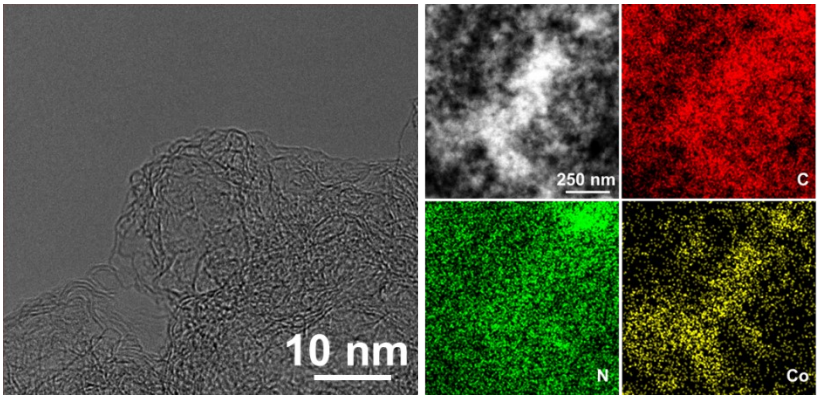

Figure S24. TEM and the corresponding EDS mapping images of PZ-POP-Co after *i-t* test.

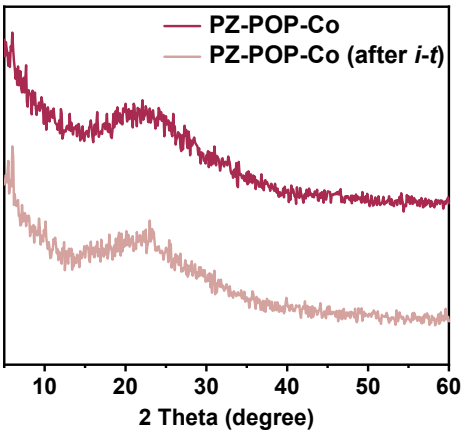

Figure S25. XRD patterns of PZ-POP-Co before and after *i-t* test.

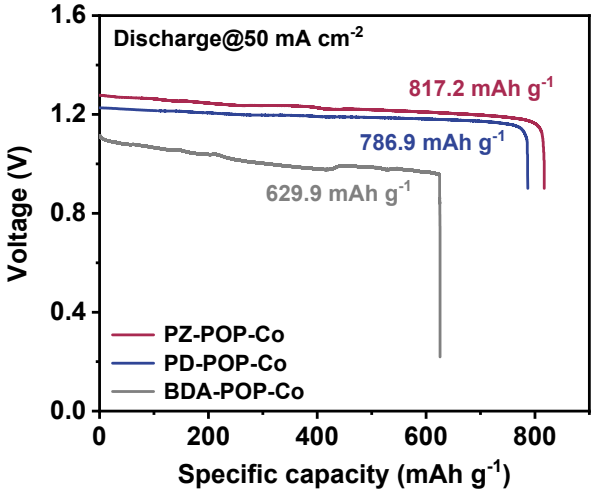

Figure S26. Galvanostatic discharge curves at the current density of 50 mA $cm^{-2}$of X-POP-Co.

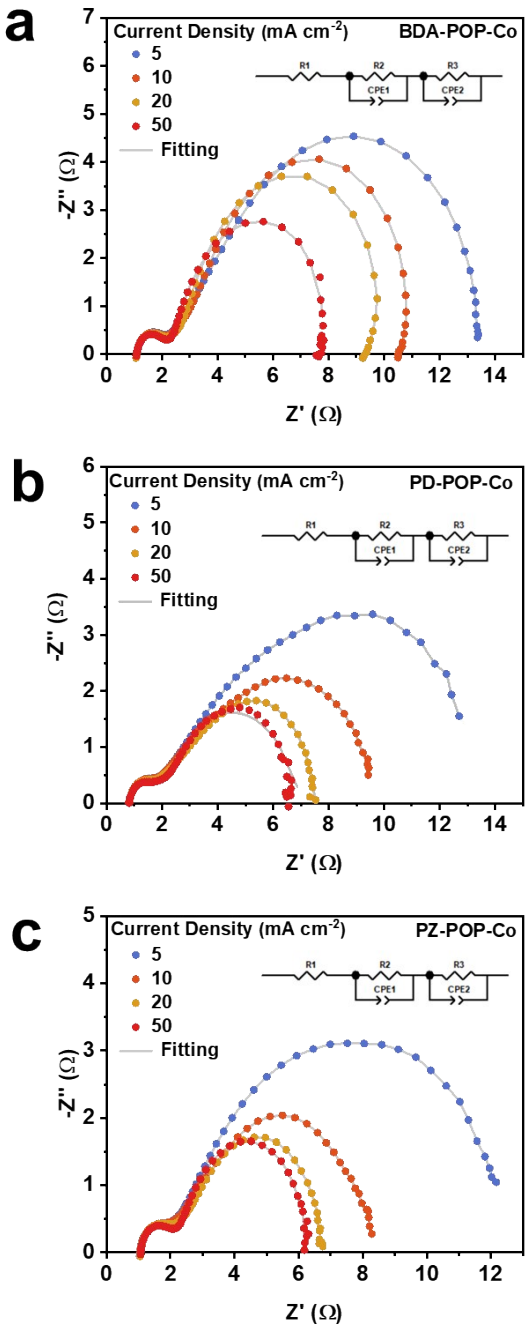

Figure S27. Nyquist plots for liquid ZABs based on **a** BDA-POP-Co, **b** PD-POP-Co and **c** PZ-POP-Co under different discharge current densities.

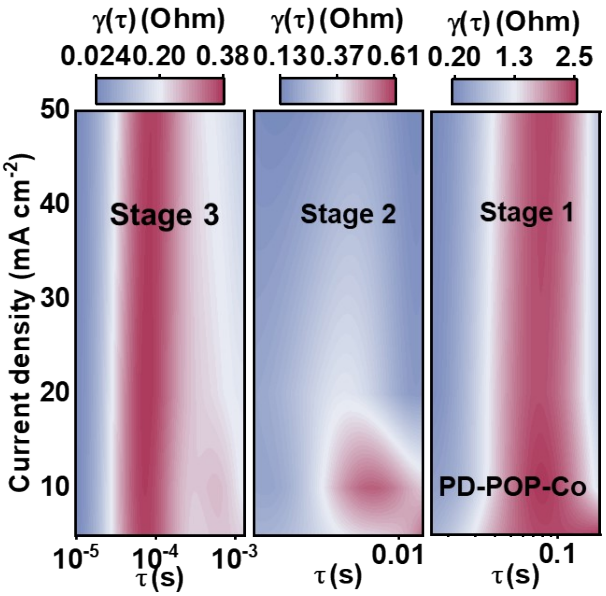

Figure S28. Contour mappings of DRT results of liquid ZAB based on PD-POP-Co.

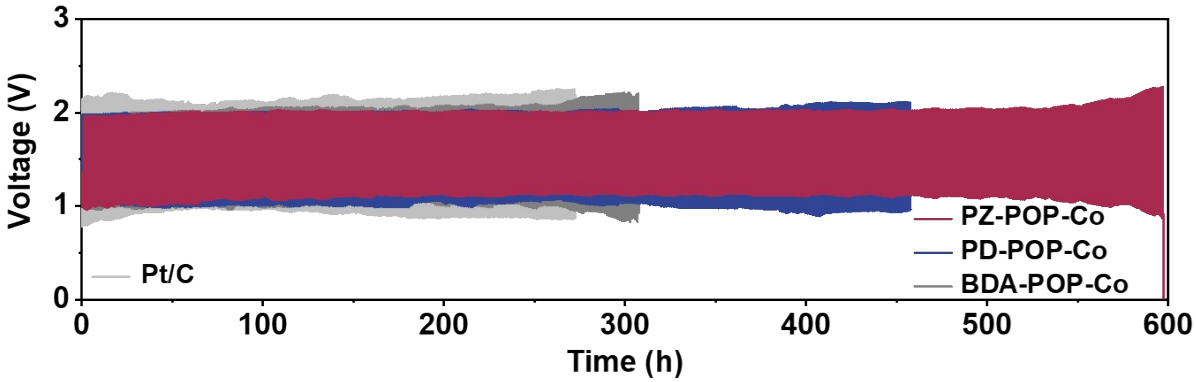

Figure S29. Galvanostatic charge/discharge cycling profiles at 20 mA cm^{-2} of ZABs with BDA-POP-Co + RuO_2, PD-POP-Co + RuO_2, PZ-POP-Co + RuO_2 and Pt/C + RuO_2 as cathode catalysts at room temperature (~25 °C).

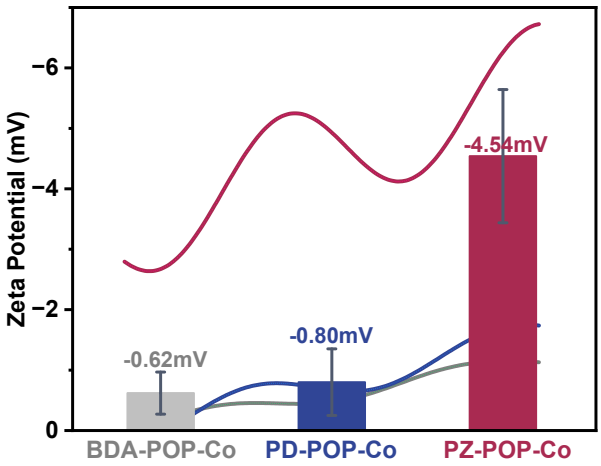

Figure S30. Zeta potential of X-POP-Co.

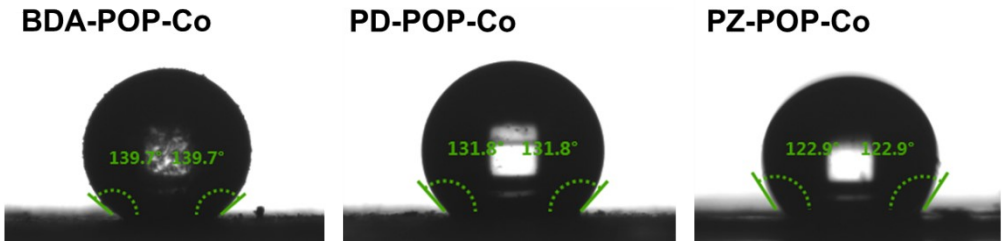

Figure S31. Water contact angles for X-POP-Co.

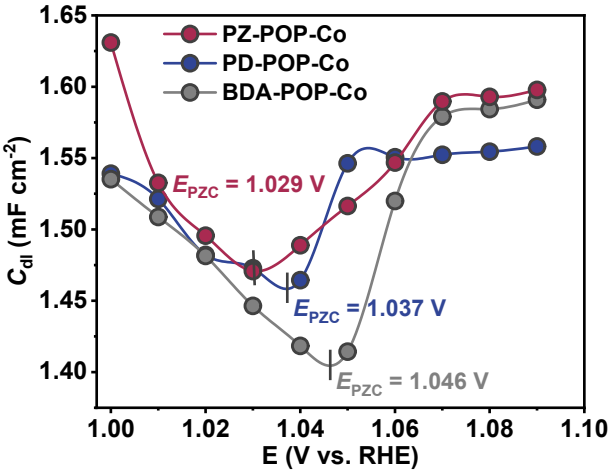

Figure S32. C_{dl} measured in 0.1 M KOH for X-POP-Co.

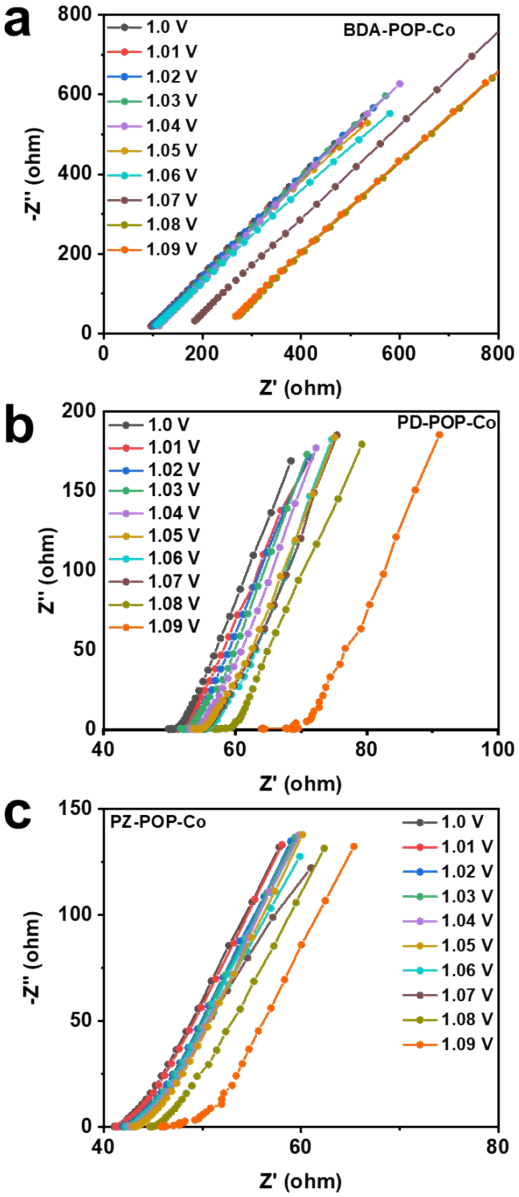

Figure S33. The Nyquist plots of **a** BDA-POP-Co, **b** PD-POP-Co and **c** PZ-POP-Co under different potentials tested in 0.1 M KOH.

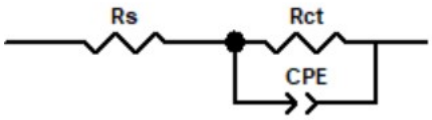

Figure S34. The equivalent circuit model, where R_s is the solution resistance, R_{ct} is the charge transfer resistance, and CPE is the constant phase element.

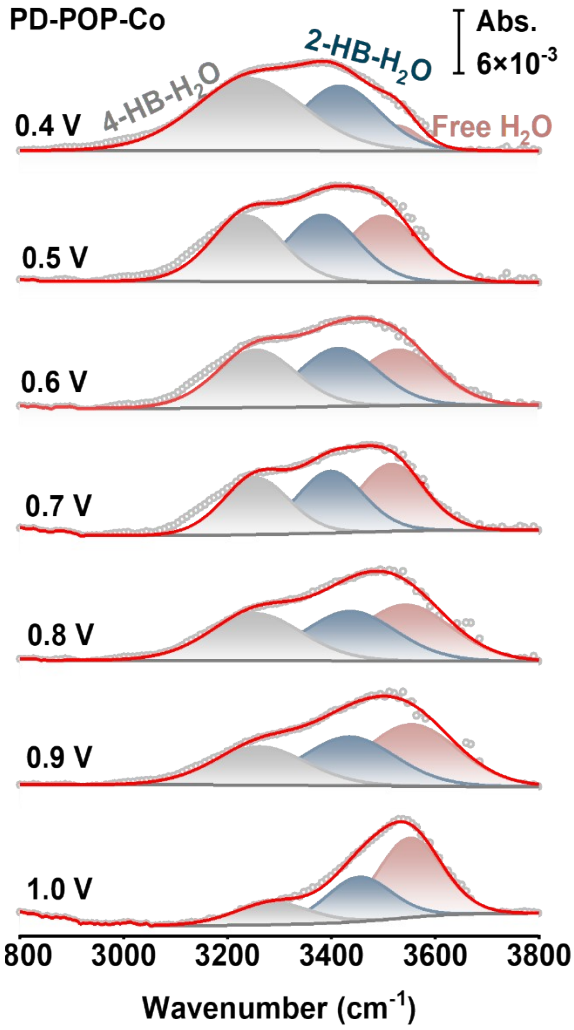

Figure S35. O-H stretching of interfacial water from *in situ* ATR-SEIRAS spectra of PD-POP-Co.

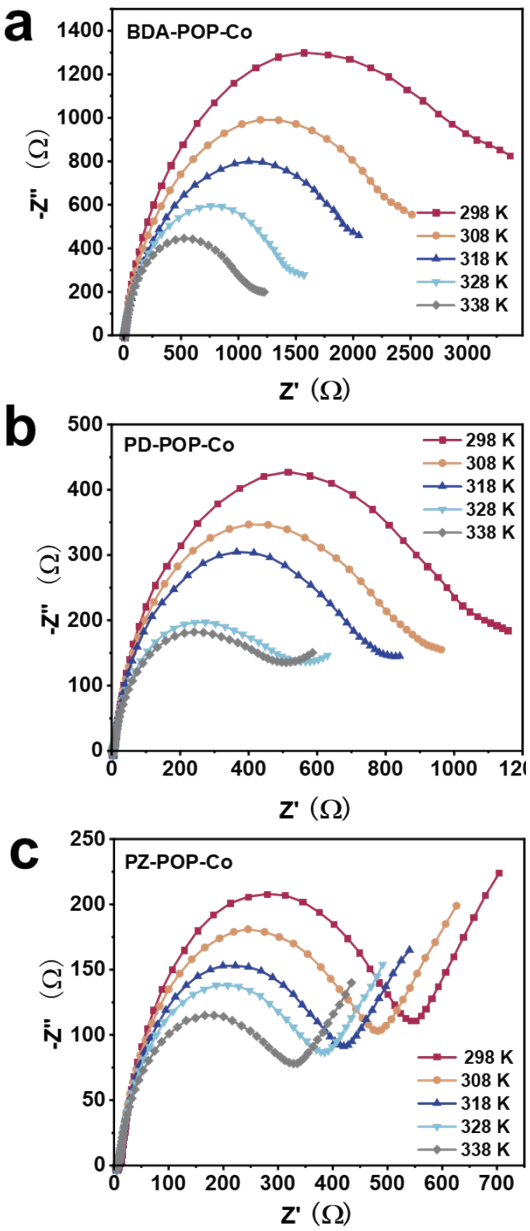

Figure S36. Nyquist plots of X-POP-Co measured at different temperatures (98% RH).

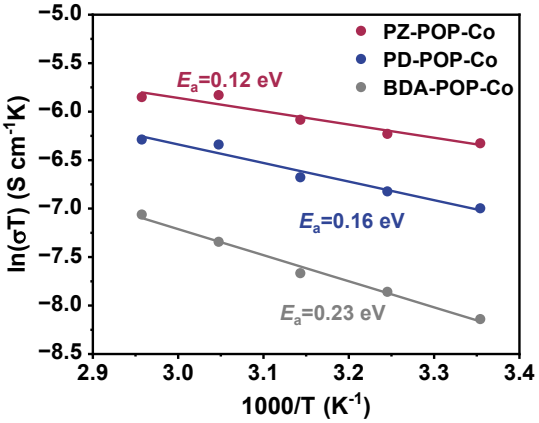

Figure S37. Arrhenius plots of X-POP-Co.

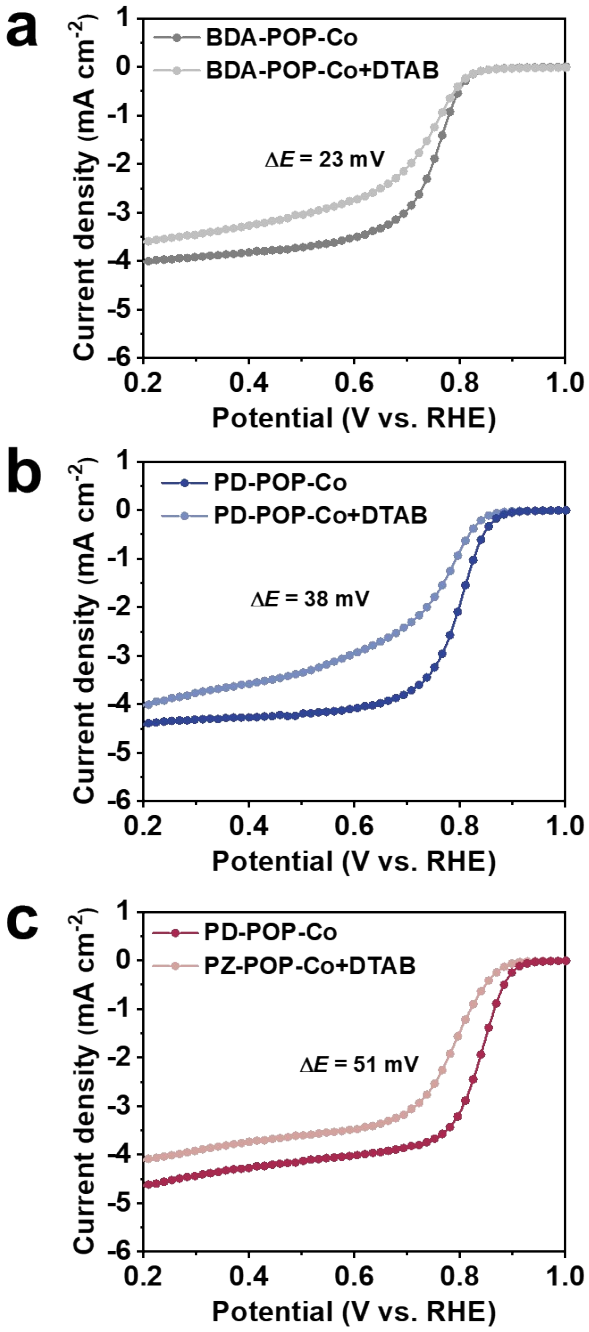

Figure S38. ORR polarization curves of X-POP-Co with and without 0.2 mM DTAB.

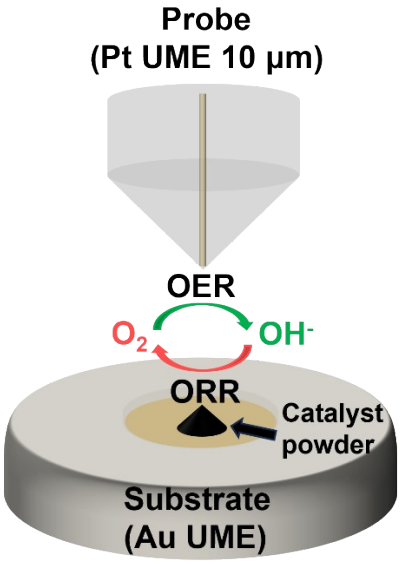

Figure S39. Setup used for a typical SECM investigation in the TG/SC mode. OER, oxygen evolution reaction.

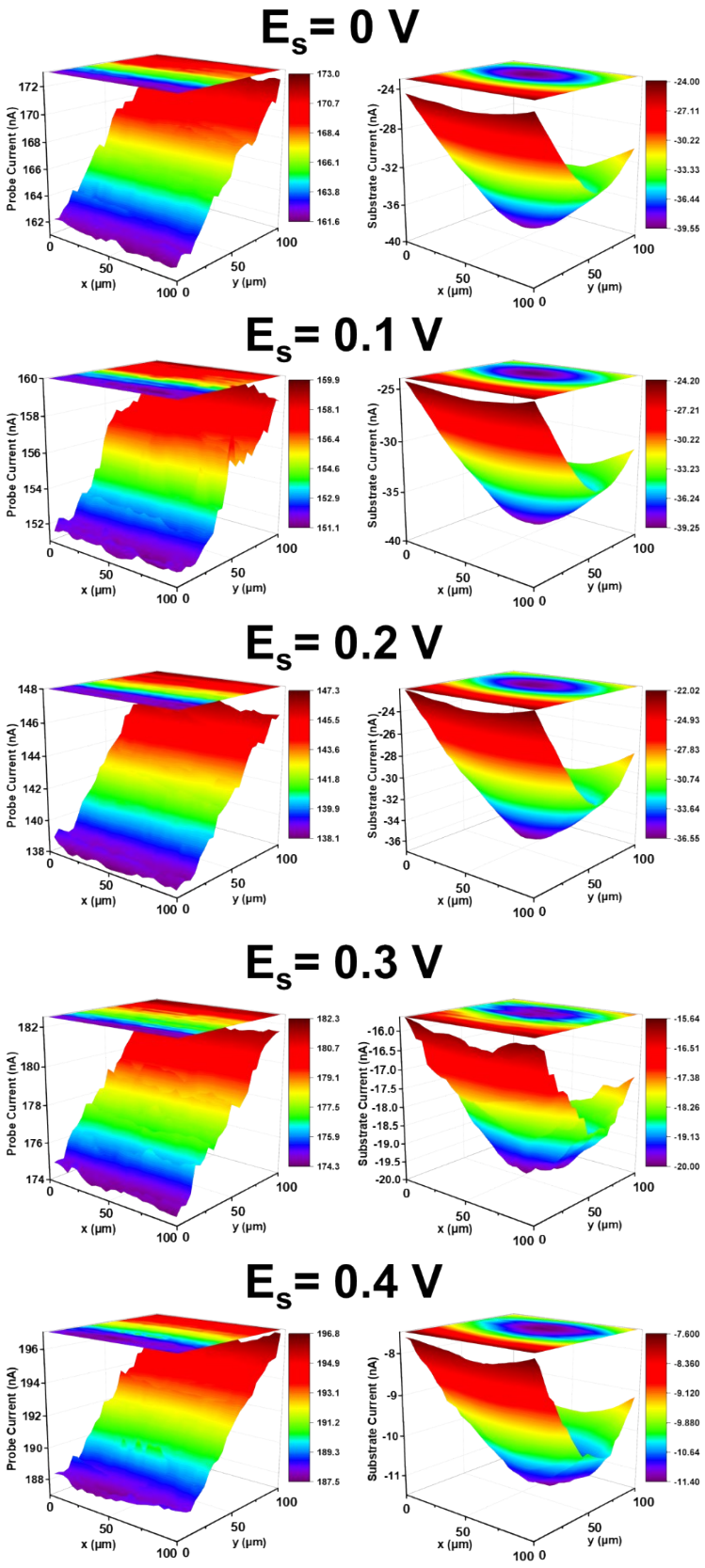

Figure S40. SECM scanning images of BDA -POP-Co at substrate potential of 0.0-0.4 V (vs. RHE). The probe is set at a certain potential of 1.8146 V (vs. RHE).

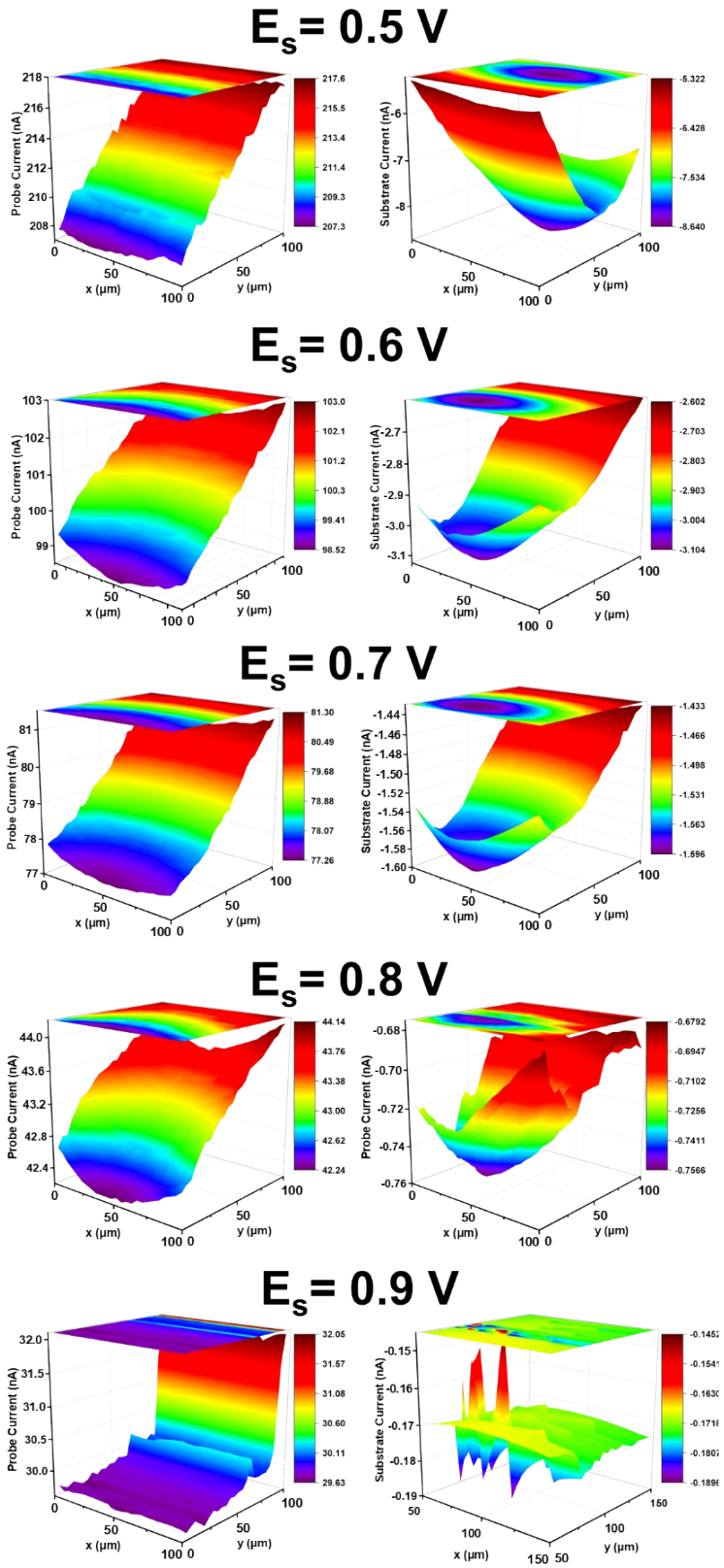

Figure S41. SECM scanning images of BDA-POP-Co at substrate potential of 0.5-0.9 V (vs. RHE). The probe is set at a certain potential of 1.8146 V (vs. RHE).

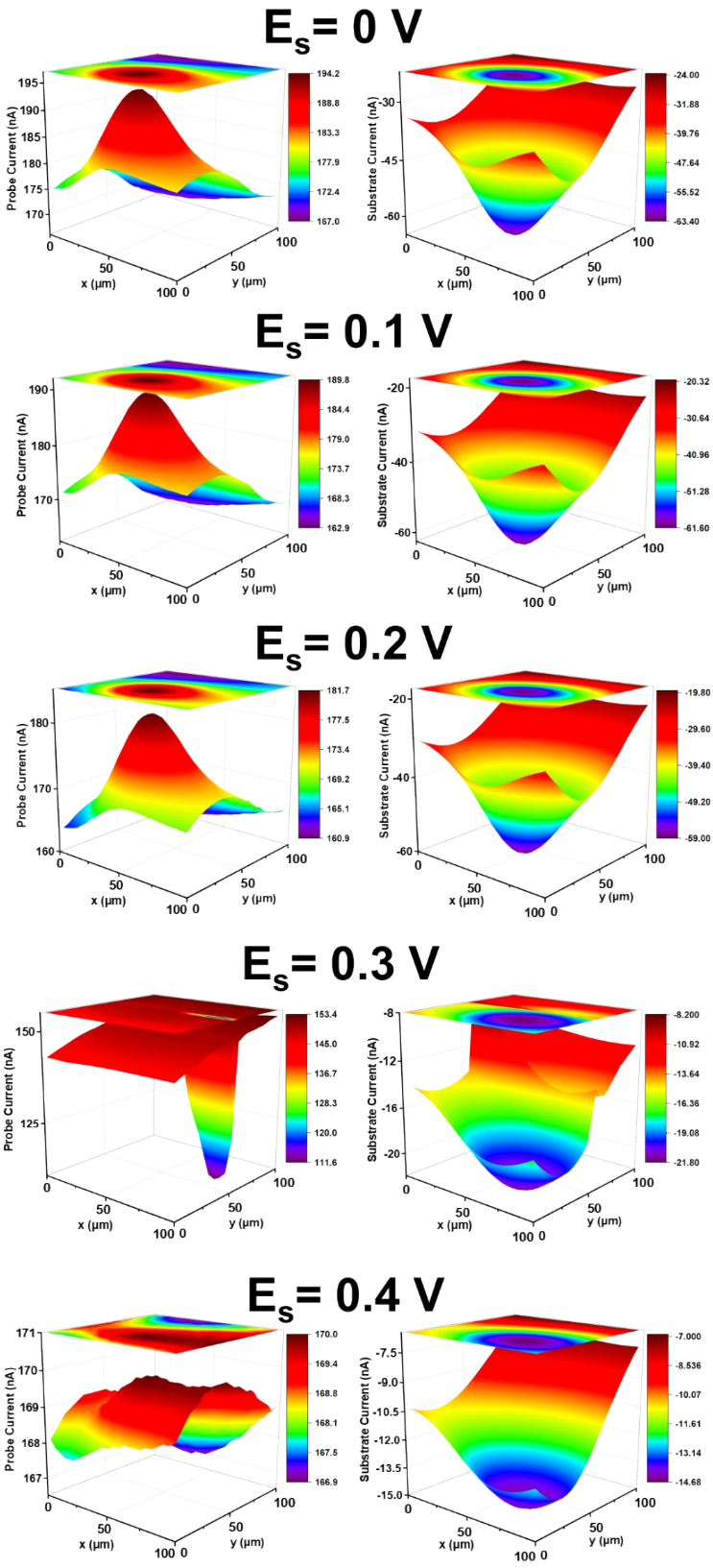

Figure S42. SECM scanning images of PD-POP-Co at substrate potential of 0.0-0.4 V (vs. RHE). The probe is set at a certain potential of 1.8146 V (vs. RHE).

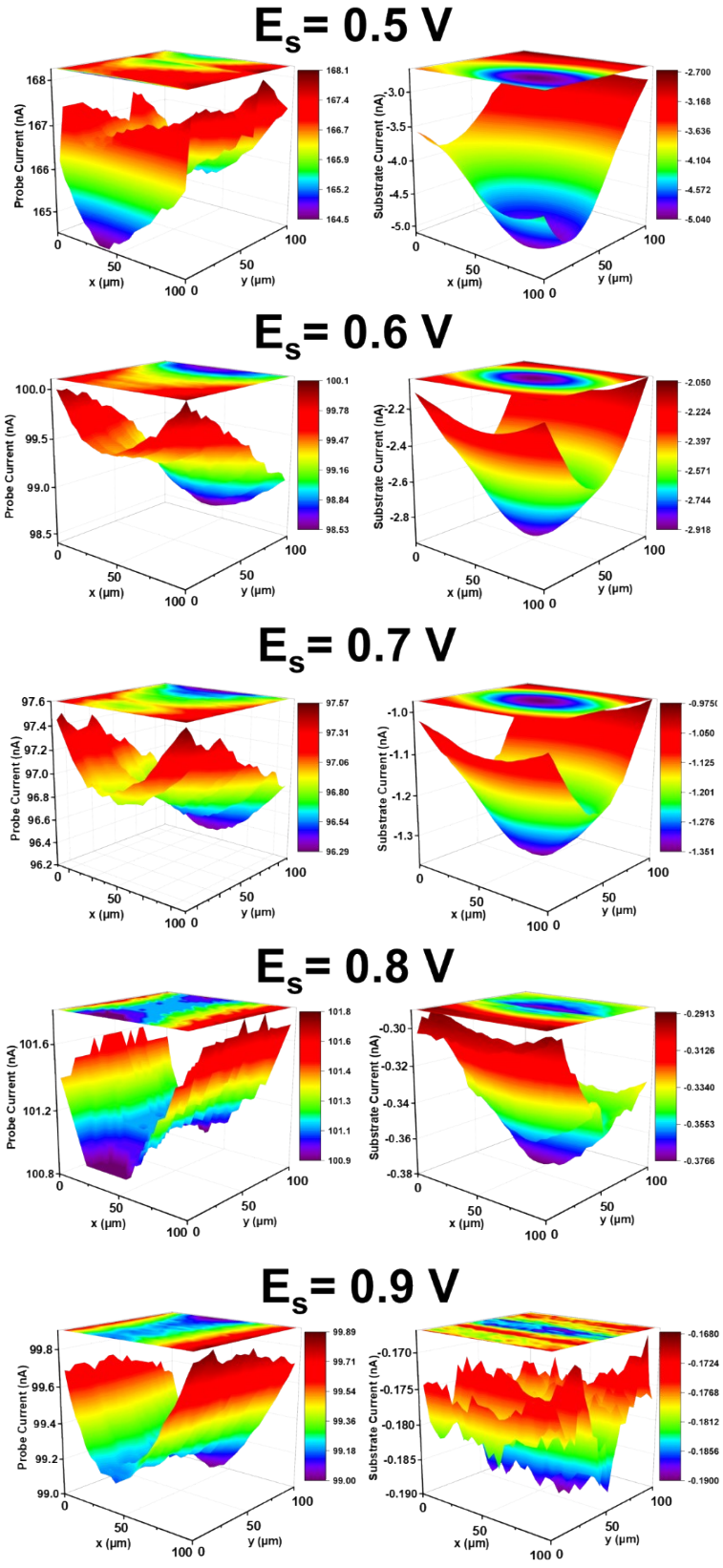

Figure S43. SECM scanning images of PD-POP-Co at substrate potential of 0.5-0.9 V (vs. RHE). The probe is set at a certain potential of 1.8146 V (vs. RHE).

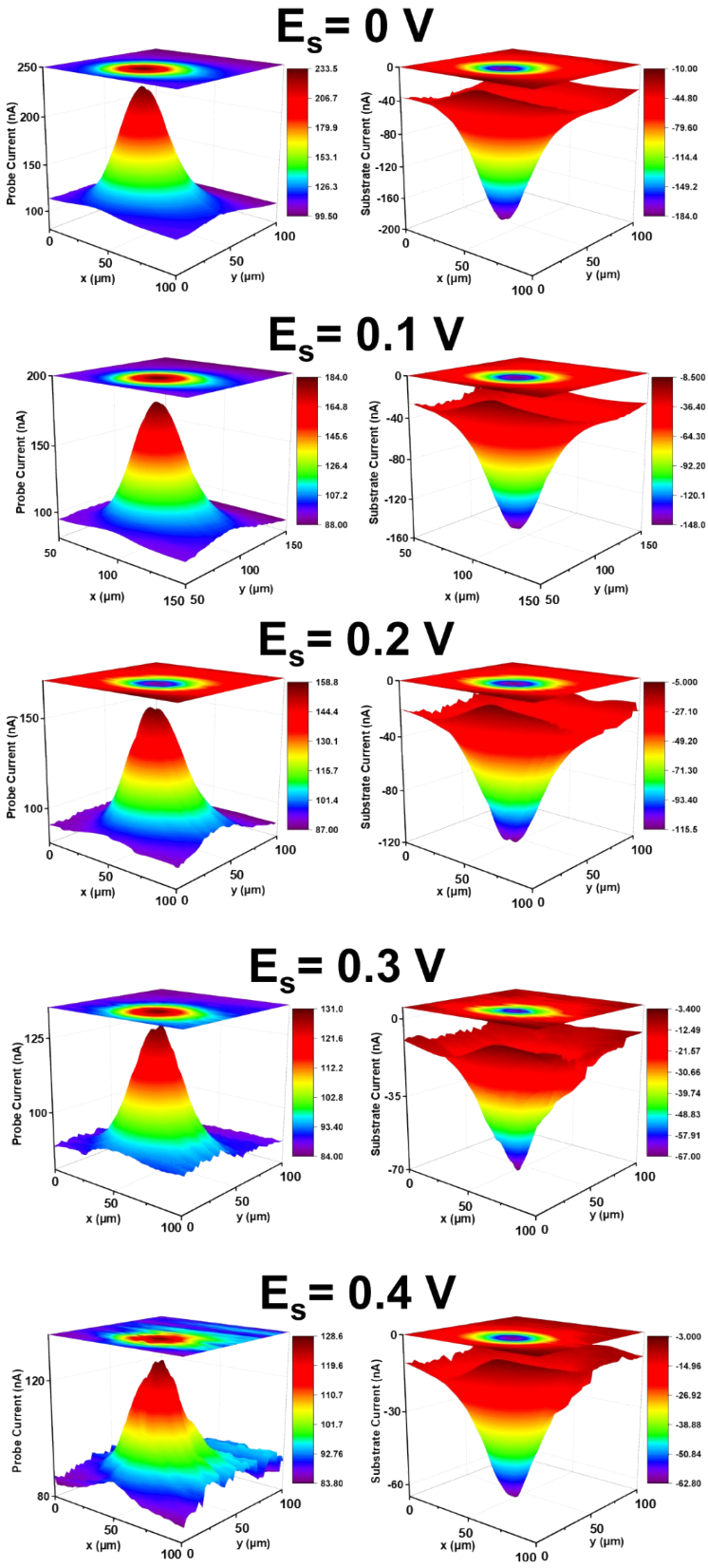

Figure S44. SECM scanning images of PZ-POP-Co at substrate potential of 0.0-0.4 V (vs. RHE). The probe is set at a certain potential of 1.8146 V (vs. RHE).

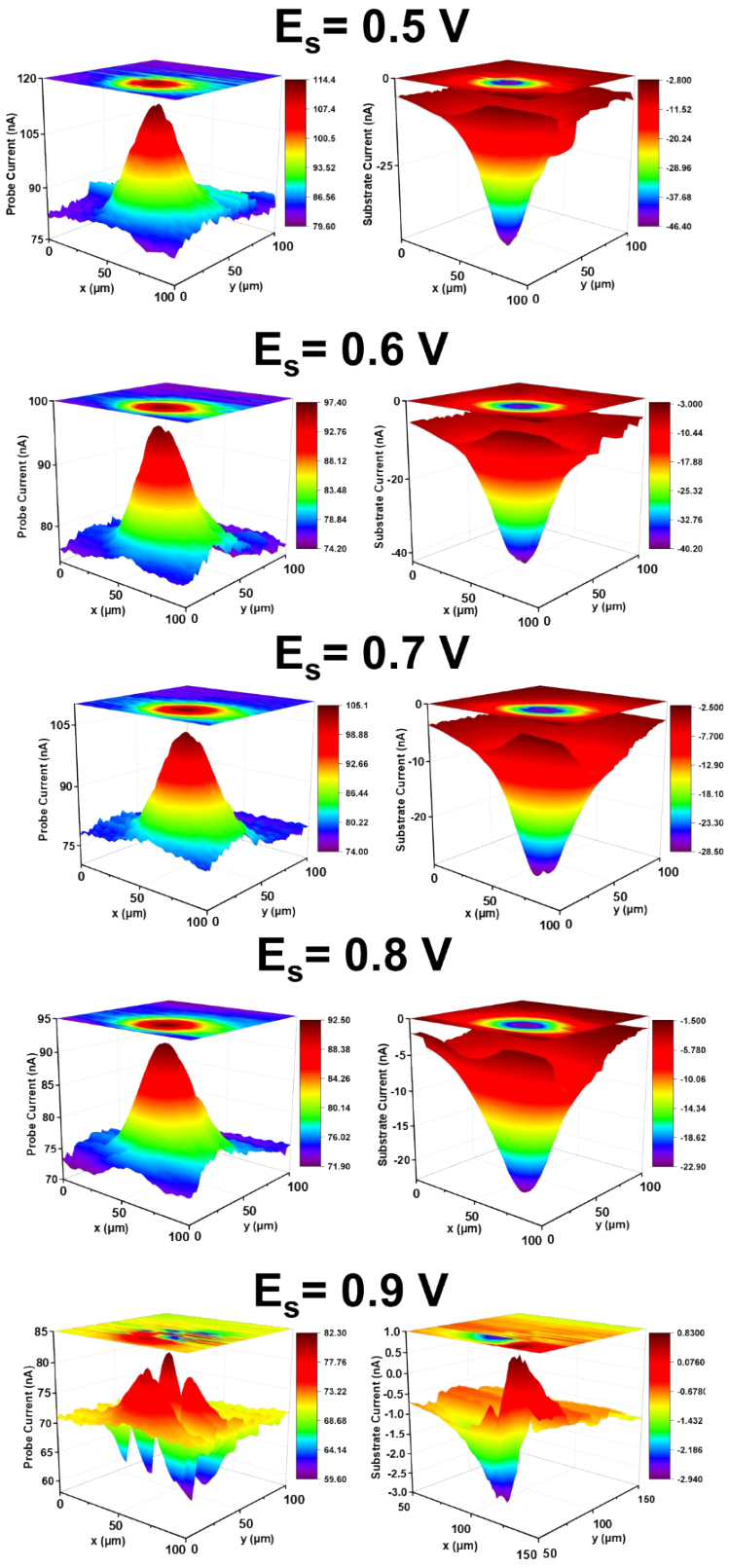

Figure S45. SECM scanning images of PZ-POP-Co at substrate potential of 0.5-0.9 V (vs. RHE). The probe is set at a certain potential of 1.8146 V (vs. RHE).

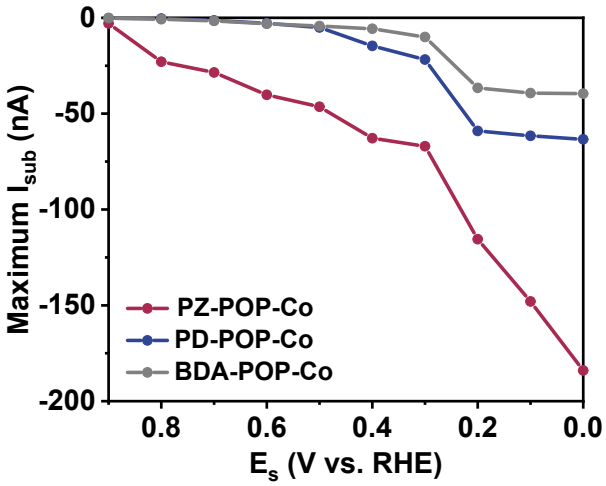

Figure S46. Plots of maximum substrate current as functions of substrate potential for SECM results.

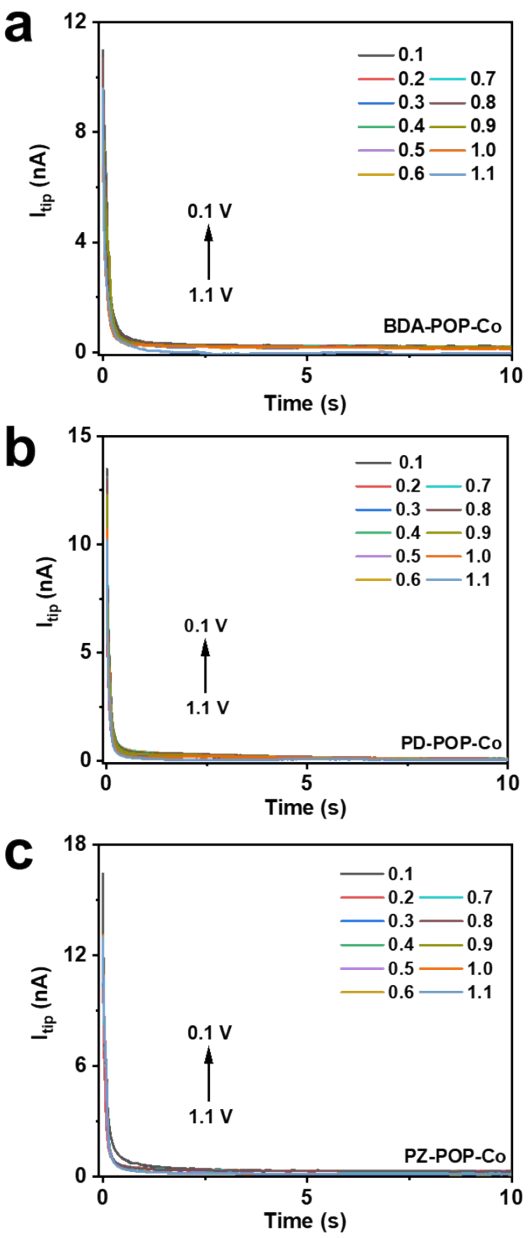

Figure S47. Chronoamperometry curves recorded on the tip in SI-SECM measurements of **a** BDA-POP-Co, **b** PD-POP-Co and **c** PZ-POP-Co.

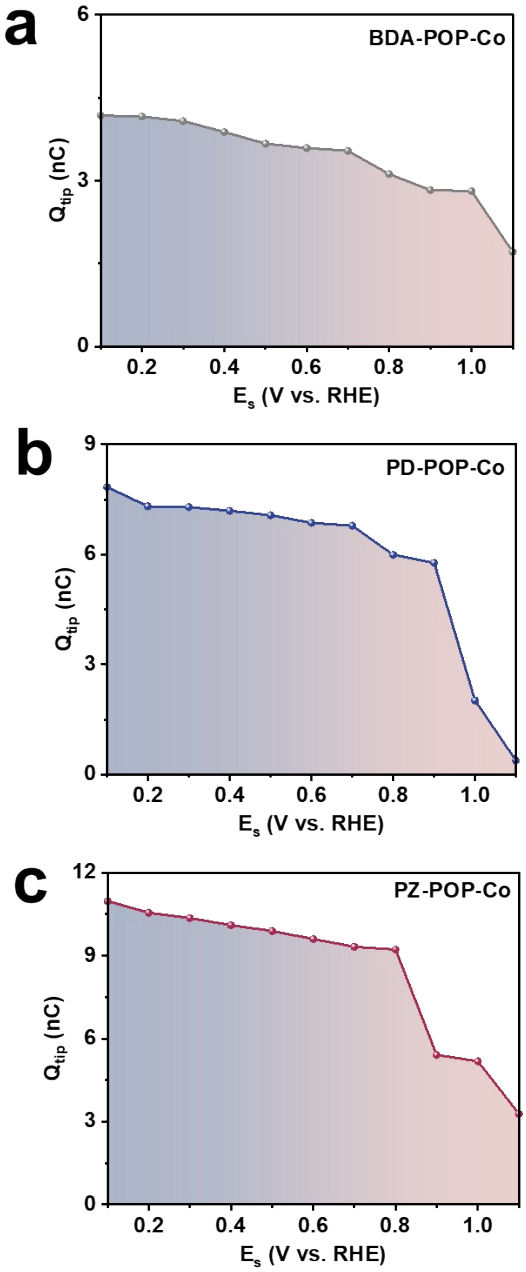

Figure S48. Integrated charge with SI-SECM for **a** BDA-POP-Co, **b** PD-POP-Co and **c** PZ-POP-Co.

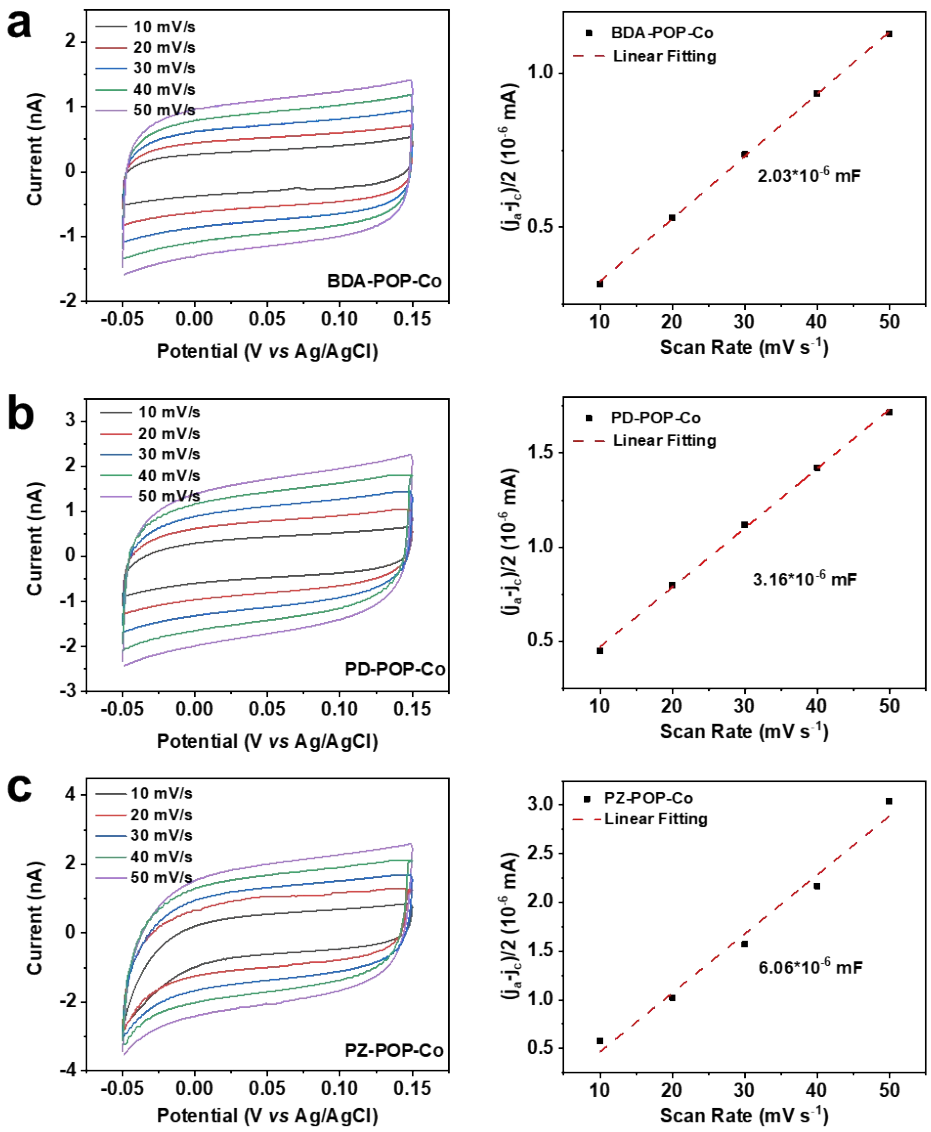

Figure S49. CV curves at different scan rates (left) and corresponding fitting results of C_{dl} (right) for **a** BDA-POP-Co, **b** PD-POP-Co and **c** PZ-POP-Co.

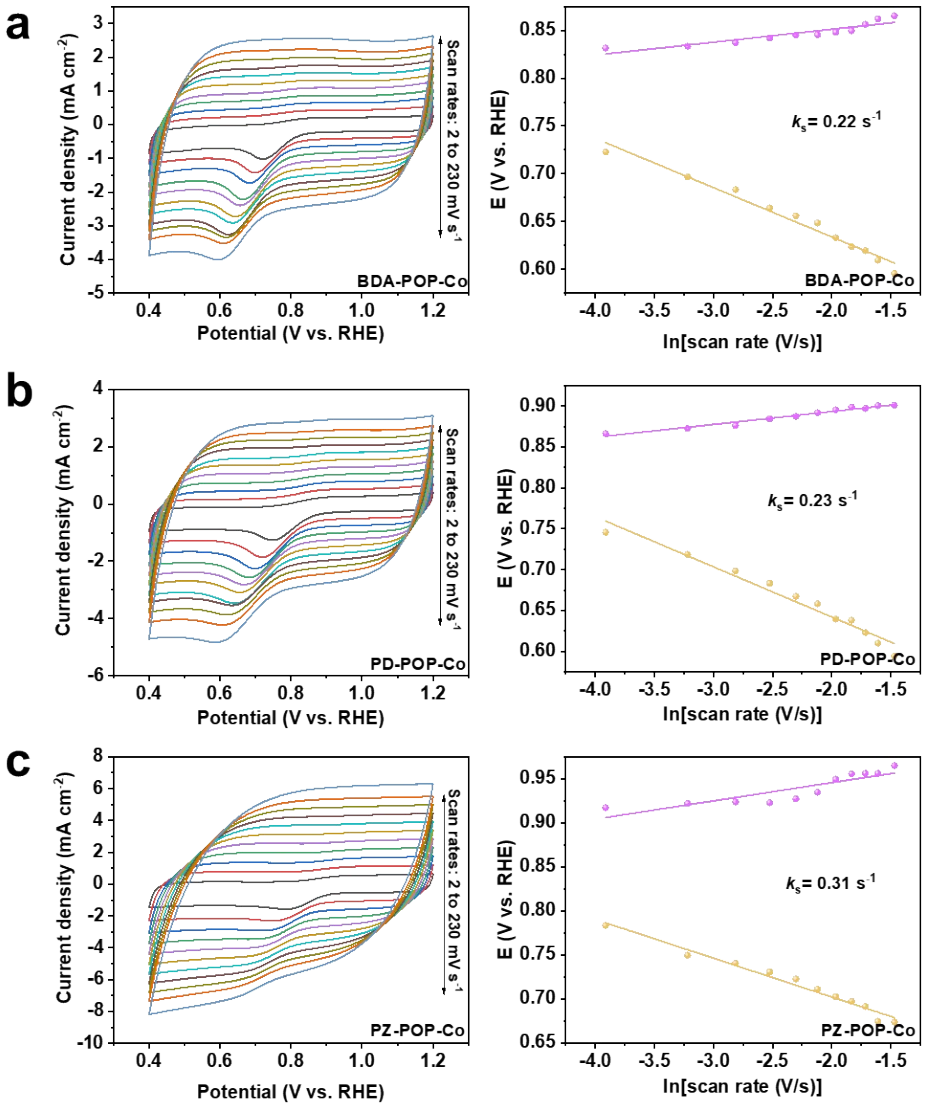

Figure S50. CV curves (left column) of **a** BDA-POP-Co, **b** PD-POP-Co and **c** PZ-POP-Co conducted in 1 mM $K_3Fe(CN)_6$/0.1 M KCl with various scan rates, and the corresponding Laviron analytical results (right column).

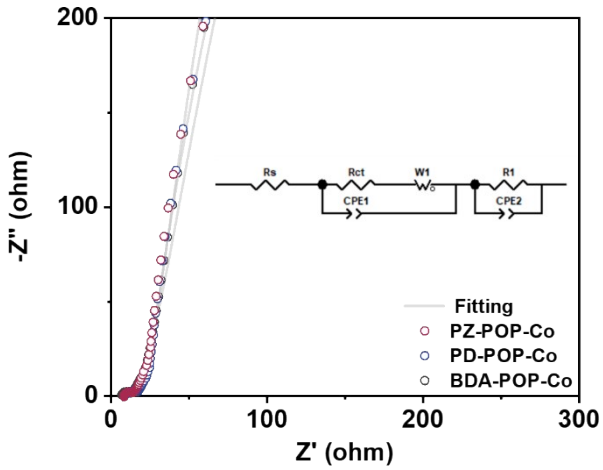

Figure S51. The Nyquist plots of X-POP-Co. Inset: the equivalent circuit for the semicircle part. The equivalent circuit model comprised solution resistance (R_s), charge transfer resistance (R_{ct}), constant phase element (CPE), and Warburg resistance for ionic diffusion (W).

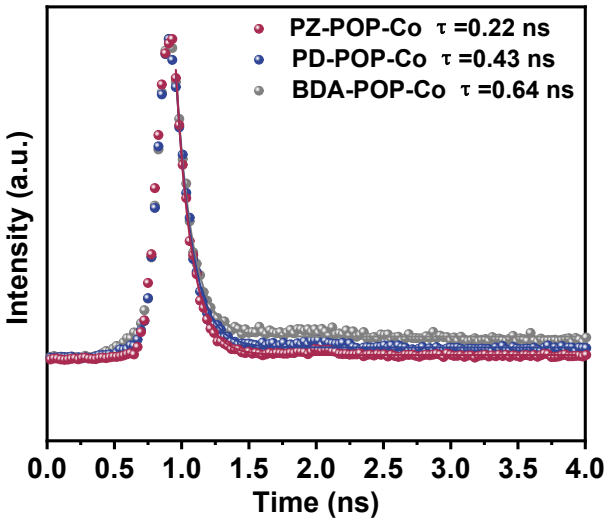

Figure S52. Fluorescent quantum lifetimes of X-POP-Co.

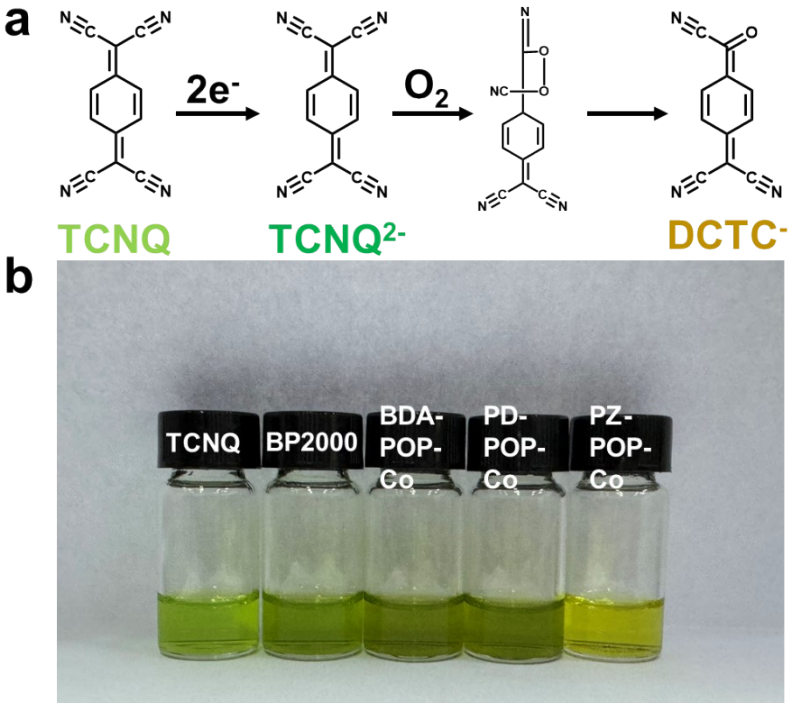

Figure S53. (a) Electron transfer reaction of TCNQ. (b) Optical image of TCNQ solutions in acetonitrile and with BP2000, BDA-POP-Co, PD-POP-Co, and PZ-POP-Co.

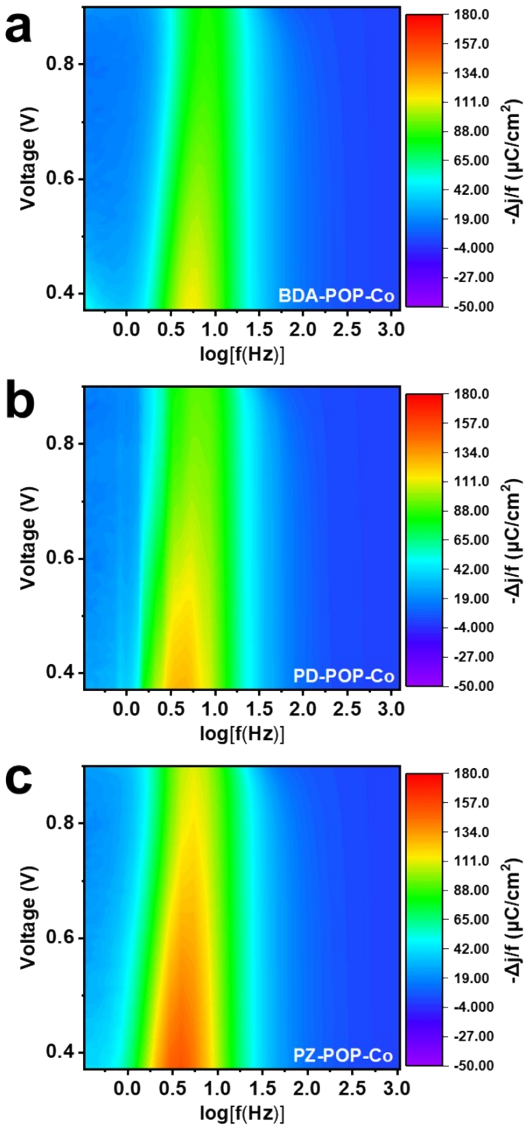

Figure S54. VF-SWV colormaps of **a** BDA-POP-Co, **b** PD-POP-Co and **c** PZ-POP-Co catalysts.

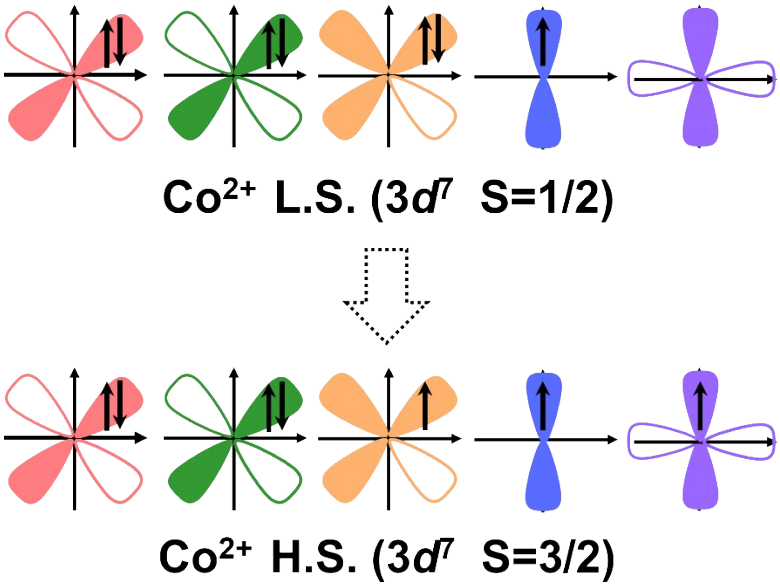

Figure S55. 3*d* electron occupations in the L.S. and H.S. states of Co^{2+} in X-POP-Co.

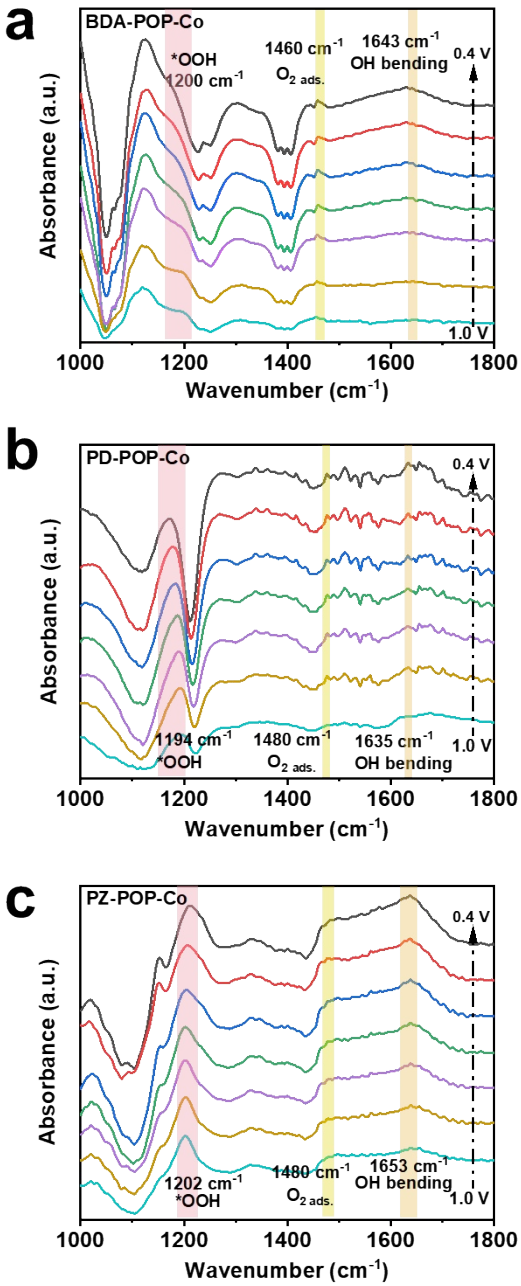

Figure S56. *In situ* ATR-SEIRAS spectra of **a** BDA-POP-Co, **b** PD-POP-Co and **c** PZ-POP-Co for ORR from 1.0 V to 0.4 V.

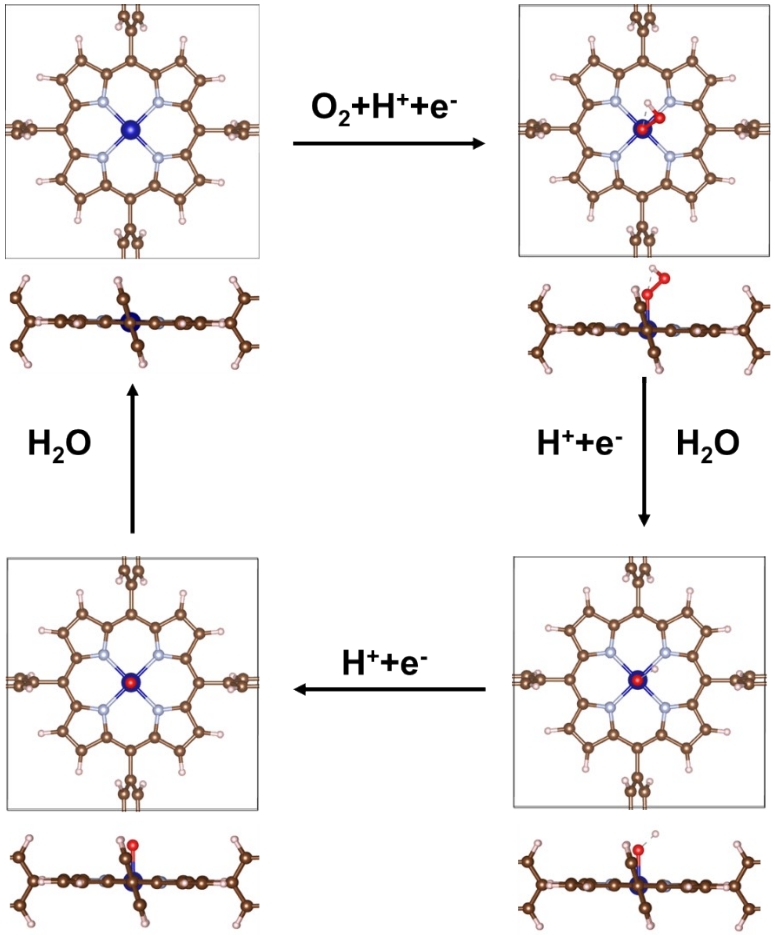

Figure S57. Side and top view of optimized adsorption configurations of each intermediate during ORR on Co-N_4 for BDA-POP-Co.

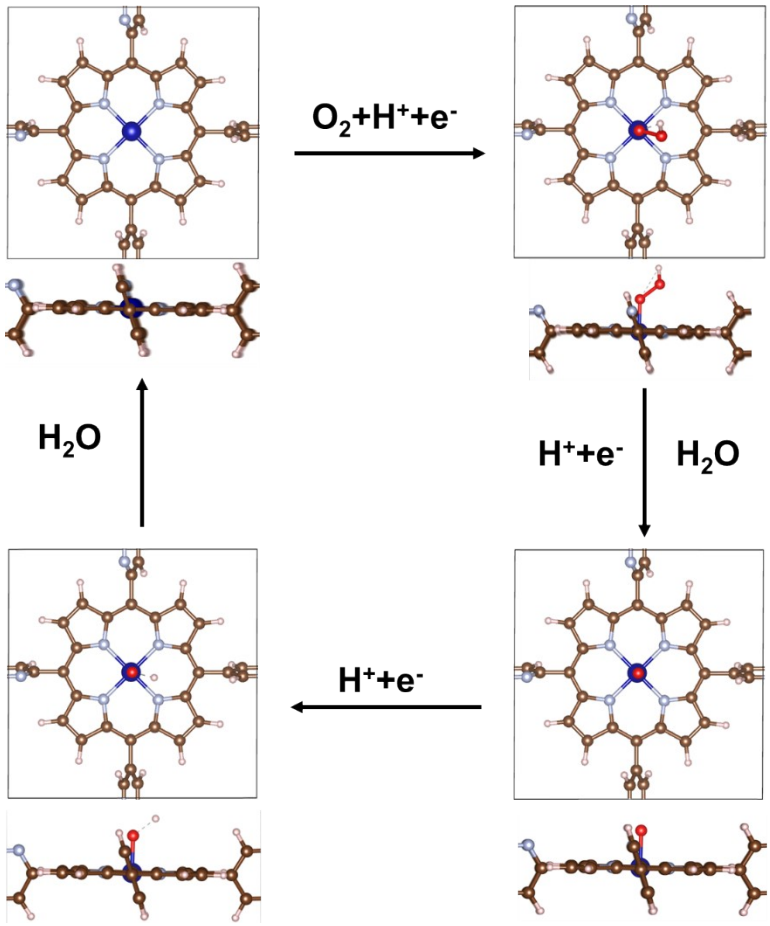

Figure S58. Side and top view of optimized adsorption configurations of each intermediate during ORR on Co-N_4 for PD-POP-Co.

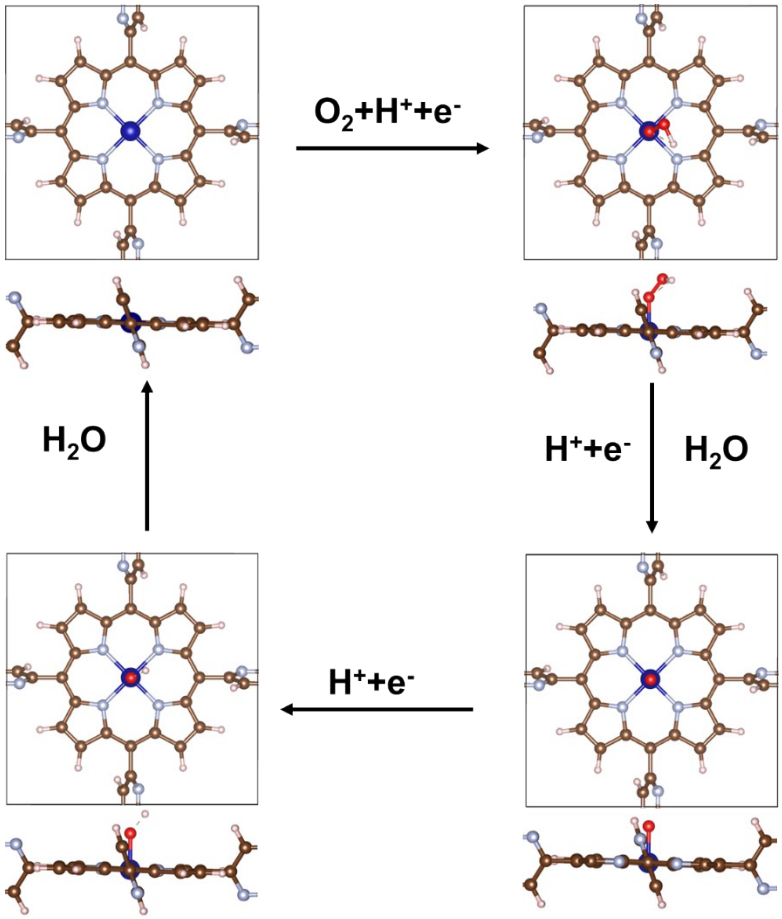

Figure S59. Top view of optimized adsorption configurations of each intermediate during ORR on Co-N_4 for PZ-POP-Co.

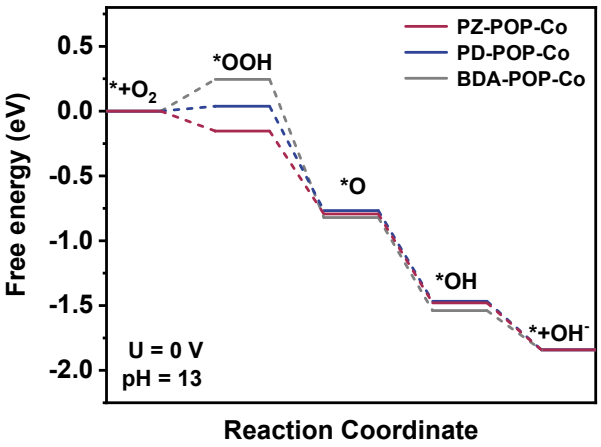

Figure S60. The Gibbs free-energy diagram of X-POP-Co analogs at $U = 0$ V.

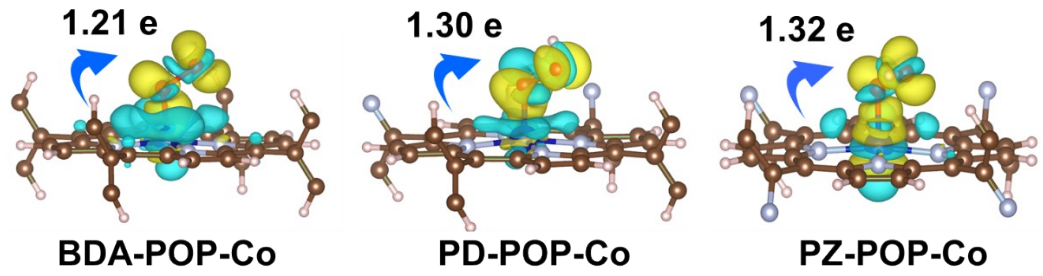

Figure S61. Charge density difference for X-POP-Co analogs at U = 0 V, pH=13.

Table S1. Summary of the Brunauer-Emmett-Teller (BET) specific surface area for X-POP-Co.

Sample	BET specific surface area (m^2 g^{-1})
PZ-POP-Co	1069.8
PD-POP-Co	1042.3
BDA-POP-Co	935.2

Table S2. Elements contents of X-POP-Co based on XPS and EDS survey.

Sample	Method	Relative amounts of elements (at.%)			
		C	N	O	Co
PZ-POP-Co	XPS	74.26	12.76	12.47	0.51
	EDS	78.69	12.34	7.92	1.05
PD-POP-Co	XPS	75.79	10.21	13.54	0.46
	EDS	81.21	10.61	7.35	0.83
BDA-POP-Co	XPS	76.79	9.59	13.2	0.42
	EDS	81.86	9.27	8.08	0.79

Table S3. Comparison of the N species of X-POP-Co.

Sample	Relative amounts of N species (%)		
	Pyrrolic N	Pyridinic N	Pyrazinic N
BDA-POP-Co	85.56	14.44	N.A.
PD-POP-Co	77.53	22.47	N.A.
PZ-POP-Co	68.17	13.21	18.80

Table S4. Summary of EIS analysis of liquid ZABs based on X-POP-Co catalysts.

Current density (mA cm^{-2})		5	10	20	25
PZ-POP-Co	R_1 (Ω)	0.7840	0.7864	0.7703	0.7713
	R_2 (Ω)	0.9972	1.009	1.293	1.293
	R_3(Ω)	11.08	6.427	4.452	4.088
PD-POP-Co	R_1 (Ω)	1.025	1.025	1.009	1.027
	R_2 (Ω)	1.023	1.131	1.395	1.246
	R_3(Ω)	14.16	8.702	5.881	5.12
BDA-POP-Co	R_1(Ω)	0.9740	0.8369	0.9237	1.013
	R_2 (Ω)	1.71	2.441	1.919	1.373
	R_3 (Ω)	11.44	7.641	7.044	5.942

Table S5. EIS fitting parameters of PZ-POP-Co in 0.1 M KOH.

E (V vs RHE)	R_s (Ω cm^2)	R_{ct} (Ω cm^2)	T (mF cm^{-2} s$^{\phi-1}$)	P	C_{dl} (mF cm^{-2})
1	42.8	8057	0.0018893	0.94488	1.631
1.01	43.38	22108	0.0018304	0.93455	1.533
1.02	45.53	75453	0.0017729	0.93672	1.496
1.03	47.52	79656	0.0017758	0.92919	1.471
1.04	41.85	41418	0.0017734	0.93702	1.489
1.05	42.03	58781	0.001752	0.94756	1.516
1.06	42.75	89804	0.0017728	0.94981	1.547
1.07	42.96	107922	0.0018189	0.94983	1.590
1.08	43.2	140790	0.0018254	0.9491	1.593
1.09	43.46	180970	0.0018267	0.94981	1.598

Table S6. EIS fitting parameters of PD-POP-Co in 0.1 M KOH.

E (V vs RHE)	R_s (Ω cm^2)	R_{ct} (Ω cm^2)	T (mF cm^{-2} s$^{\phi-1}$)	P	C_{dl} (mF cm^{-2})
1	58.72	24818	0.00188745	0.9152	1.539
1.01	68.52	25544	0.00186087	0.91101	1.521
1.02	51.77	48363	0.00184378	0.915	1.482
1.03	51.18	58259	0.00181349	0.91954	1.472
1.04	53.08	69363	0.00180208	0.91881	1.464
1.05	51.42	80345	0.00188022	0.9228	1.546
1.06	53.17	102690	0.001890037	0.92069	1.551
1.07	54.4	398430	0.00189688	0.9189	1.552
1.08	56.04	336960	0.00189901	0.91799	1.554
1.09	55.55	189730	0.00189709	0.91957	1.558

Table S7. EIS fitting parameters of BDA-POP-Co in 0.1 M KOH.

E (V vs RHE)	R_s (Ω cm^2)	R_{ct} (Ω cm^2)	T (mF cm^{-2} s$^{\phi-1}$)	P	C_{dl} (mF cm^{-2})
1	73.97	24180	0.00182847	0.91976	1.535
1.01	73.6	23587	0.00179993	0.91982	1.509
1.02	71.12	24522	0.00177441	0.91992	1.481
1.03	82.13	22208	0.00176123	0.90773	1.446
1.04	87.49	23929	0.00172119	0.90744	1.418
1.05	95.7	21923	0.00172364	0.90133	1.414
1.06	161.5	28275	0.00172135	0.91176	1.519
1.07	238	39467	0.00173363	0.90516	1.579
1.08	235	42264	0.00172255	0.91581	1.584
1.09	231	40546	0.00174005	0.91099	1.590

Table S8. Relative proportions of 4-HB-H_2O of X-POP-Co.

E (V vs RHE)	PZ-POP-Co	PD-POP-Co	BDA-POP-Co
0.4	37.86	48.34	22.06
0.5	35.99	32.9	21.76
0.6	35.52	33.58	21.48
0.7	34.13	30.5	21.23
0.8	34.99	30.71	19.67
0.9	34.76	25.82	21.54
1.0	34.63	17.13	15.95

Table S9. Relative proportions of 2-HB-H_2O of X-POP-Co.

E (V vs RHE)	PZ-POP-Co	PD-POP-Co	BDA-POP-Co
0.4	35.99	36.5	35.91
0.5	34.5	33.76	35.38
0.6	36.03	33.92	35.18
0.7	35.11	33.32	34.73
0.8	35.32	32.45	33.83
0.9	35.17	32.74	33.57
1.0	35.04	29.8	15.19

Table S10. Relative proportions of free H_2O of X-POP-Co.

E (V vs RHE)	PZ-POP-Co	PD-POP-Co	BDA-POP-Co
0.4	26.15	15.15	42.03
0.5	29.51	33.74	42.86
0.6	28.45	32.5	43.34
0.7	30.76	36.18	44.04
0.8	29.68	36.84	46.5
0.9	30.07	41.44	44.89
1.0	30.33	53.07	68.86

Table S11. Summary of EIS analysis of X-POP-Co catalysts.

Sample	R_s (Ω)	R_{ct} (Ω)
PZ-POP-Co	6.367	3.63
PD-POP-Co	8.617	5.50
BDA-POP-Co	9.044	6.84

Table S12. Calculated *d*-band center of X-POP-Co.

Sample	$\varepsilon_{d\ spin\text{-}up}$ (eV)	$\varepsilon_{d\ spin\text{-}down}$ (eV)	ε_{d} (eV)
PZ-POP-Co	-0.77078	-0.18207	-0.47642
PD-POP-Co	-0.90399	-0.60324	-0.75361
BDA-POP-Co	-0.68963	-0.64766	-0.65264

References

1. T. H. Wan, M. Saccoccio, C. Chen and F. Ciucci, *Electrochimi. Acta.* 2015, **184**, 483-499.
2. G. Kresse and J. Hafner, *Phys. Rev. B.* 1994, **49**, 14251-14269.
3. G. Kresse and J. Furthmüller, *Phys. Rev. B.* 1996, **54**, 11169-11186.
4. J. P. Perdew and Y. Wang, *Phys. Rev. B.* 1992, **45**, 13244-13249.